Fault Roughness and Fault Complexity

Field Study, Multi-Scale Analysis and Numerical Fault Model

Dissertation

zur

Erlangung des Doktorgrades (Dr. rer. nat.)

der

Mathematisch-Naturwissenschaftlichen Fakultät

der

Rheinischen Friedrich-Willhelms-Universität Bonn

vorgelegt von

Martin Navarro

aus

Manapla, Philippinen

Bonn, Juni 2002

Angefertigt mit Genehmigung der Mathematisch-Naturwissenschaftlichen Fakultät der Rheinischen Friedrich-Willhelms-Universität Bonn

1. Referent: Prof. Dr. H. J. Neugebauer
2. Referent: Prof. Dr. N. Froitzheim

Tag der Promotion: 18. Juli 2002

Abstract

We study the roughness of normal faults in lignite and its relevance to the complex process of faulting by means of field observations and a numerical model for wear at rough fault surfaces. Roughness data is collected at field scale for which only sparse information is available today. A multi-scale analysis of the data is used to scan for characteristic scales of processes.

Field investigations, multi-scale analysis, and numerical fault model draw a consistent picture of fault evolution. In a first stage, processes like coalescence of fractures and non-planar fault propagation form a rough fault. In the following stage, characteristic scales of damage are introduced by the offset of rough fault surfaces. The model shows that the geometrical aspects of fault roughness alone are able to produce non-trivial damage characteristics. Roughening and smoothening processes freely modify fault roughness perpendicular to slip direction. This process holds on as long as there is a permanent input of large-scale roughness during fault growth. The possible relevance of this structural self-organization for slip dynamics is discussed.

With respect to fault complexity, the observed processes introduce different mechanisms of scale coupling that unfold a multi-scale pattern of fault related structures. The spectrum of scales covered by the evolution of fault structures is both continuous and discontinuous depending on scale and location. The relevance of the findings for observing and modeling faulting processes are discussed.

Zusammenfassung

Die vorliegende Arbeit beschäftigt sich mit der Rauhigkeit geologischer Störungen und dem Zusammenhang zwischen Rauhigkeit und struktureller Störungskomplexität. Hierzu wurden in einem Tagebau mehrere Abschiebungen innerhalb der Braunkohle untersucht. Durch eine Multiskalen-Analyse der Rauhigkeit werden charakteristische Prozeßskalen identifiziert. Ein numerisches Modell zur Reibung rauher Störungsflächen wird vorgestellt, um den Einfluß der Rauhigkeit auf die Störungsentwicklung zu untersuchen.

Die Geländebefunde, die Multiskalen-Analyse und das numerische Modell zeichnen ein konsistentes Bild der Störungsentwicklung. In einem ersten Stadium wird durch Verschmelzen von Brüchen und unebene Bruchausbreitung eine rauhe Störung gebildet. Im folgenden Stadium leitet die Verschiebung der rauhen Bruchflächen Zerrüttungsprozesse auf charakteristischen Skalen ein. Die Ergebnisse der numerischen Modellierung zeigen, daß eine multiskalige Rauhigkeit genügt, um ein nichttriviales Muster an Zerrüttungstrukturen zu erzeugen. Dies wird dadurch hervorgerufen, daß Aufrauhungs- und Glättungsprozesse

die Störungsfläche senkrecht zur Bewegungsrichtung frei verändern. Die Relevanz dieser Selbstorganisation der Rauhigkeit für die Störungsdynamik wird diskutiert.

Die beobachteten Prozesse stellen verschiedene Mechanismen der Skalenkopplung im komplexen System einer Störung bereit. Sie erzeugen ein Muster an Strukturen, das einen weiten Skalenbereich umfaßt. Das Skalenspektrum der Strukturen kann in Abhängigkeit von Ort und Skala sowohl kontinuierlich als auch diskontinuierlich erscheinen. Die Relevanz dieses Befundes für die Beobachtung und Modellierung von Störungen wird diskutiert.

Acknowledgments

I want to thank Prof. Dr. H.-J. Neugebauer for the outstanding working conditions and for leading me to an overall sight when I stuck in the details. I want to thank Dr. S. Hergarten for his permanent readiness to discuss and for leading me to the details when I stuck in the overall sight. Many thanks to the mining company *Rheinbraun AG* for the ample support of the field survey, especially to Mr. Schulz, Mr. Hartung, Mr. Asmus, Mr. Diederich, and Mr. Gerdom; but there are still many others whose help is greatly appreciated. I want to thank Prof. N. Froitzheim for his expert opinion on this study. Without my colleagues, I would have grown lonely; so many thanks to them, too.

Contents

1 Introduction **11**
- 1.1 Complexity of faults . . . 11
- 1.2 Scale coupling and fault roughness . . . 13
- 1.3 Linking multi-scale roughness with processes . . . 13
- 1.4 Aims of the study . . . 16

2 Geological setting and data acquisition **17**
- 2.1 Outcrop overview . . . 17
- 2.2 Data acquisition . . . 21
- 2.3 Reference surfaces for fault roughness . . . 23

3 Field observations **25**
- 3.1 Characteristics of fault roughness . . . 25
  - 3.1.1 Segmentation . . . 25
  - 3.1.2 Incorporated joints . . . 25
  - 3.1.3 Arcuate segments . . . 27
  - 3.1.4 Vertical roughness . . . 29
- 3.2 Damage phenomena induced by fault roughness . . . 32
  - 3.2.1 Large splay faults and associated damage . . . 32
  - 3.2.2 Fault wall damage at the m-scale . . . 35
- 3.3 Discussion . . . 44

4 Multi-scale analysis of fault traces **45**
- 4.1 Measuring roughness . . . 45
- 4.2 Fractal analysis . . . 47
  - 4.2.1 Method . . . 47
  - 4.2.2 Results . . . 48
  - 4.2.3 Discussion . . . 51

4.3 Characteristic scales . . . 52
4.3.1 Isotropic roughness measure . . . 52
4.3.2 Results . . . 52
4.3.3 Discussion . . . 55

5 Numerical fault model **57**
5.1 Purpose . . . 57
5.2 Physical description . . . 59
5.3 Model simplification . . . 61
5.4 Numerical model . . . 66
5.5 Parameter space . . . 68
5.6 Results . . . 70
5.6.1 Central parameter set . . . 70
5.6.2 Variation of grid size . . . 73
5.6.3 Variation of relative strain . . . 74
5.6.4 Variation of relative yield slope . . . 76
5.6.5 Variation of Hurst exponent . . . 77
5.6.6 Variation of lubrication . . . 77
5.6.7 Comparison with field and experimental data . . . 79
5.7 Discussion . . . 80

6 Conclusions **83**
6.1 Fault evolution and scale interaction . . . 83
6.2 Friction and slip dynamics . . . 84

7 Relevance for the approach to complex geosystems **87**
7.1 On recognizing and monitoring geosystems . . . 87
7.2 On modeling geosystems . . . 88
7.3 Can we understand geosystems? . . . 90

Bibliography **90**

Chapter 1

Introduction

1.1 Complexity of faults

What is a fault? In textbooks we usually find a fault defined as a fracture having appreciable movement to the plane of the fracture. In some cases, this provides a quite acceptable understanding of what a fault is, but the definition is a very strong idealization of the natural phenomena. A fault looking like a single shear surface at map scale reveals a wealth of localization and deformation structures when it is inspected in field. The scale range at which strain and displacement localization takes place reaches down to the granular and even molecular scale. In contrast to the primary definition, the global shear deformation does not localize to a single fracture but forms a vast assembly of shear zones covering a multiplicity of scales. Not only the structure of a fault is complex; also the dynamics of faulting, controlled by a variety of interacting factors like rock rheology, stress, temperature, and fluid pressure exhibit high complexity. This makes clear why the phenomenon of faulting eludes a clear definition. Especially if more than macroscopic features of a fault are relevant to a process, as it is the case for questions concerning seismicity and fluid flow, the simple fault definition given above looses relevance. The focus then shifts towards the aspect of complexity.

Faults are prime examples for complex systems in the earth sciences. The science of complexity has evolved during the past century and has grown to a multidisciplinary field of research during the past 15 years. Definitions of complex systems are numerous, perhaps because they have to deal with such different aspects as, for example, algorithmic computability, biological organisms, social interplay, and geosystems. Yet, there is some consensus about the key ingredients of complex systems in nature.

Natural complex systems are composed of a large number of elements that interact lo-

cally. Faults for example evolve through the local interaction of grains or molecules of a rock. The key characteristics of a complex system is the self-organization of an overall behavior which is not determined by the properties of the constituents and their local interactions. This phenomenon of "the whole being more than the sum of the parts" is called *emergence*. In case of faults, the evolving structural and deformational patterns are an emergent property of the rock body that is not predictable on the basis of the local interactions of molecules. This unpredictability is attributed to a system behavior that produces order but is chaotic to a certain degree. We recognize faults because we recognize the order of structure, but we are not able to predict the detailed position and appearance of localization zones. Even if the overall behavior of the system can be predicted statistically, the details of the system remain unpredictable. Chaotic behavior is introduced by a non-linearity of the local interactions. A solid body under stress, for example, has no complex behavior as long as stresses remain within the range of linear elasticity. If growth of microcracks is stimulated, the evolution of fracture patterns will introduce complexity into the mechanical reaction of the rock body. The local break down of molecule bonds along cracks produces a non-linear dependency between strain and stress at the molecule scale.

Complex geosystems self-organize multi-scale patterns in time or space domain, which means that many time or space scales are needed to describe the behavior of the system. The term *scale* can either refer to a sample size or sample resolution at which the fluctuation of a system property is observed, or it can refer to an object size if the property forms objects, i.e. spatial or temporal clusters that can be well distinguished from each other. The type of scale used to describe stress fields, for example, usually is a sample size or sample resolution, whereas structural features of a fault are usually described by object scales because the displacement field shows distinct clusters that can be identified as faults, joints, microcracks or other structures (this is the effect of localization). Why complex geosystems form multi-scale patterns cannot be explained by the concept of local interaction between a vast amount of small elements. A process description at the element scale does not comprise any information about the formation of patterns. This is the phenomenon of emergence. It is not enough to consider processes at a single scale to understand why a complex geosystem reacts on such a broad scale range. If, on the other hand, processes are investigated at multiple scales, we find a coupling of process scales that is able to explain the formation of multi-scale patterns. Scale coupling means that processes on a certain scale are influenced by processes on sub or super-scales and cannot be sufficiently explained without this influence. The development of a shear zone, for example, is controlled by interaction of shear zones and fractures at a sub-scale and will appear spontaneous if it is observed without considering the sub-scale. Scale influence can be mutually leading to scale interaction and introducing feedback to the system. Crack coalescence, for example, influences the development of structural patterns on a super-scale whereas these patterns locally promote or inhibit crack growth on the sub-

scale. Due to scale coupling with limited spatial or temporal sphere of influence, the system unfolds patterns in scale space. An approach to complex systems therefore must include a consideration of the mechanisms of scale coupling.

1.2 Scale coupling and fault roughness

Faults can be described by the spatial and temporal variations of stress or strain fields. Geological interpretation favors a more structural view on faults because structures are both conserved and easy to detect. The difference between both points of view is that the one focuses on structural entities and the other on the properties that lie in between. Since this study is concerned with field data, it will consider structural aspects of faults and follow the question, how structures can induce scale coupling processes.

There are two major processes which introduce coupling of scales. The first is the process of fracture or fault nucleation by means of fracture growth and coalescence. This leads to the formation of rough fractures or shear zones on increasing length scales. Structures of different scales influence each other mutually during fracture growth. A large fractures, for example, inhibits the growth of smaller fractures in its environment. The second process is the generation of small-scale structures by a large fracture or shear zone. The macroscopic stress field acting on the structure leads to local stress concentration at sub-scales. There are mainly two sources of stress concentration. The first is the concentration at the so called ”process zone” around the tip of a fracture or shear zone (Moore and Lockner 1995). The process zone propagates together with the crack tip and leaves behind a trace of damaged rock composed of small-scale discontinuities. The second source is the stress concentration induced by interlocking asperities. In order to maintain slip, asperities are forced to fail, which may also affect wide parts of the host rock. Fracture generation at the sub-scale can influence the mechanical properties of the macroscopic fracture.

These processes are able to generate structural patterns that cover a broad scale range. Apparently, fault roughness is a central parameter: it is both a record of pattern formation controlled by fracture interference at sub-scales and an agent for pattern formation controlled fractures at super-scales. We will therefore focus on fault roughness as a key parameter for the investigation of scale coupling related to faulting.

1.3 Linking multi-scale roughness with processes

How does roughness evolve and how does roughness influence the faulting process? A broad range of scales has to be considered when relating fracture geometry to fracturing processes.

Hence, we will first take a look at the scaling characteristics of roughness before we turn to the possibilities of process identification.

For simplicity, let us assume that fracture surfaces can be represented by a one- or two-dimensional function of surface height. On average, amplitudes of roughness (height differences) will increase if the observation scale (distance between two observation points) is increased. Sometimes it can even be noticed that, independent of scale, a constant magnification of amplitudes is achieved when the scale of observation is increased by a constant factor. This kind of scale invariance is called *fractal scaling* and can be described by a power-law dependency between scale δ and amplitude A by $A \sim \delta^b$ with $b > 0$. Fractal scaling of fractures was first investigated by Mandelbrot et al. (1984) who applied the theoretical framework of fractal geometry to experimental fractures in aluminum alloy. Since then, many experimental studies have concentrated on the scaling of roughness. It was shown that fracturing processes can produce crack surfaces that obey fractal scaling laws within broad scale ranges. Some researchers even state *universal* scaling laws in the sense that the power-law exponent b does not depend on material and fracture mode (Bouchaud et al. 1990, Måløy et al. 1992, Poon et al. 1992, McAnulty et al. 1992, Schmittbuhl et al. 1993, 1995, López and Schmittbuhl 1998). Progress has been made in understanding the growth of fractal crack surfaces. It was possible to show that fractal scaling can be generated by a moving crack front whose roughness evolves due to random pinning obstacles (Halpin-Healey and Zhang 1995, Barabaasi and Stanley 1995, Bouchaud 1997). All this seems to approve the fractal nature of fractures. Yet, fractal scaling was mostly observed at experimental fractures generated at laboratory scale. On the contrary, natural fractures and faults can show significant deviations from fractal scaling. Frequently, a scale dependency of the scaling exponents is found (Brown and Scholz 1985a, Power et al. 1987, Lee and Bruhn 1996). This might indicate that faulting processes are more complicated in nature than in the laboratory. There are some reasons why the scaling behavior of natural fractures and faults is still not well understood.

- Roughness data is still sparse at the field scale, i.e. in the scale range between several meter and several 100 m because good outcrop conditions are very rare at these scales.

- It is difficult to find the processes responsible for the scaling characteristics of roughness. Scale dependencies of the scaling exponent have been assumed to stem from grain sizes or preferential scales of processes, such as wear, fracture coalescence or weathering. However, a scaling exponent is not a reliable indicator for a faulting process. Different processes might produce similar exponents, and a scaling exponent might be a product of a compound process.

- Common measures of roughness, such as the *variogram*, *root mean square roughness*, and *power spectral density* produce ambiguous results for natural fractures. These

measures are suited to determine the fractal properties of functions generated by the process of *fractional Brownian motion* (fBm), which are commonly assumed to be similar to fracture topography, but it is unclear how meaningful measurements of fractal characteristics are if they are applied to non-fractal topographies. Especially functions with internal structure can bias the interpretation toward fractal scaling (Figure 1.1). In fact, many faulting processes are known to generate fault segmentation, i.e. internal structure. Segall and Pollard (1980) and Willemse (1996), for example, describe how fault segmentation develops due to coalescence of isolated fractures, such as microcracks, joints, faults, or isolated fingers of a propagating fault front (Peacock 1991, Peacock and Sanderson 1991, Shen et al. 1995). Further on, lithological inhomogeneities (Childs et al. 1996), changing stress conditions, or slip on layer boundaries (Watterson et al. 1998) can lead to fault segmentation.

What does this mean for the identification of roughening processes? Firstly, more data has to be collected at field scale. Secondly, the attempt of process identification should not be restricted to the investigation of scaling laws but should also take structural aspects into account. This can be accomplished by measures of roughness which have been adapted for structure identification. The determination of *process scales* implies that characteristic scales of roughness can be attributed to specific faulting processes found in the field. Information about process scales can also be provided by a size-statistics of specific segmentation structures but in many cases structure conservation and identification proves problematic.

The other major task is to investigate the influence of roughness on faulting processes. Again, a broad range of roughness scales has to be considered. Modeling roughness as a multi-scale phenomenon requires large computational resources. This is a severe problem if the faulting process of interest requires a three-dimensional representation of the rock body, which itself needs a lot of computational power. In consequence, studies considering multi-scale roughness mostly focus on secondary fault properties which can be described in two dimensions, such as hydraulic permeability of a single fracture(Brown 1987), closure (Brown and Scholz 1985b, 1986), normal stress distribution (Hansen et al. 2000) or shear strength (Seidel and Haberfield 1995, Yang and Chen 1999). Models of faulting processes that allow for a multi-scale roughness are forced to the same two-dimensional view and to strong idealizations of fracture mechanics, like, for example, the simple analytical and kinematical models of Scholz (1987) and Hallgass et al. (1997) for wear and seismic slip. A likely reason why the influence of multi-scale roughness on fault evolution is still weakly investigated is that such brute simplifications appear to be intolerable to most researchers. However, they are necessary if the influence of multi-scale roughness on fault evolution shall be investigated numerically.

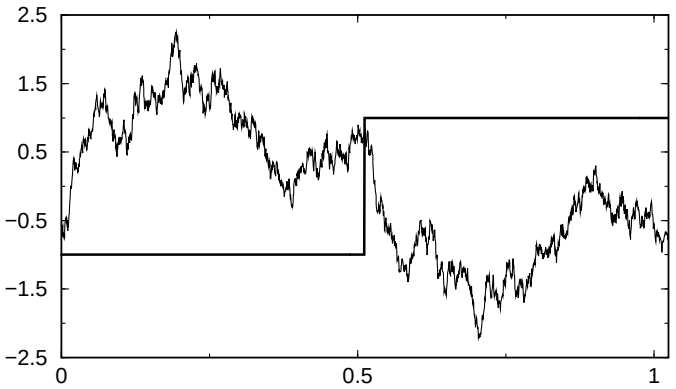

Fig. 1.1: A non-fractal square-signal and a fractal function generated by fractional Brownian motion. Both have the same power spectral density, i.e. an identical roughness according to this measure. The structure information of the square-signal is hidden in the phase information which is lost during the calculation of the spectral power.

1.4 Aims of the study

In this study, processes of structure formation related to the multi-scale roughness of faults shall be investigated by means of field observations and a numerical fault model. The relevance of the investigated processes for scale coupling and slip dynamics shall be discussed.

Qualitative and quantitative field data are collected from normal faults in lignite in an open cast lignite mine. Horizontal profiles of rough faults were sampled at field scale (1 cm to 330 m), a scale range for which only few data is available today. Both borders of the fault gouges were sampled to obtain additional information for process identification. A multi-scale analysis of roughness will be used to scan for characteristic scales of processes. A numerical model for wear between rough fault surfaces will be introduced to investigate the influence of fault roughness on damage and to explain the field observations.

The field observations are presented in chapter 3; chapter 4 deals with the multi-scale analysis of fault traces, and the numerical fault model is introduced in chapter 5. Conclusions for scale coupling and slip dynamics are drawn in chapter 6. The relevance of the findings for the approach to complex geosystems is discussed in chapter 7.

Chapter 2

Geological setting and data acquisition

2.1 Outcrop overview

Synsedimentary normal faults are studied in the open-cast lignite mine Hambach, which is located in the Lower Rhine Graben in Germany. The area of investigation is situated on the Erft-block, 4 km away from the Rur-fault, which is the prominent fault structure of the area (Figure 2.1). In the mine, a layered sequence of tertiary sands, clays, silts, and lignite is cut by a system of synsedimentary normal faults. Sand is the predominant lithology of the sedimentary record and mostly unconsolidated. There is some evidence that faulting took place at shallow depths because there is no significant hiatus in the overlying strata whose thickness does not exceed 250 m.

Most of the displacement of a fault is distributed over a narrow *shear zone* that comprises a multiplicity of subordinate shear surfaces. The appearance of the shear zone largely depends on the lithology of the fault walls. Shear zones which emerge in sand beds have a width of a few millimeters to centimeters. Observation is facilitated because dilated sands of the shear zone are bleached by migrating fluids that have washed off bituminous particles from the grains. If a sand bed forms one fault wall and lignite the other, the sand takes over most of the throw due to the stiffness of the lignite. The shear zone broadens and splits into a network of minor shear surfaces (Figure 2.2). Shear zones which develop solely in lignite are very different from this. Fault walls appear as almost rigid plates enclosing a highly mobile *fault gouge* composed of clay, silt or lignite fragments. In the outcrops, the width of the shear zone varies between 1 mm and approximately 2 m (Figure 2.3). Possible reasons for this variation will be discussed below.

If a clay layer is faulted, the shear zone can contain substantial amounts of clay smear in the range between the separated parts of the clay bed. Sandy clay and silt layers con-

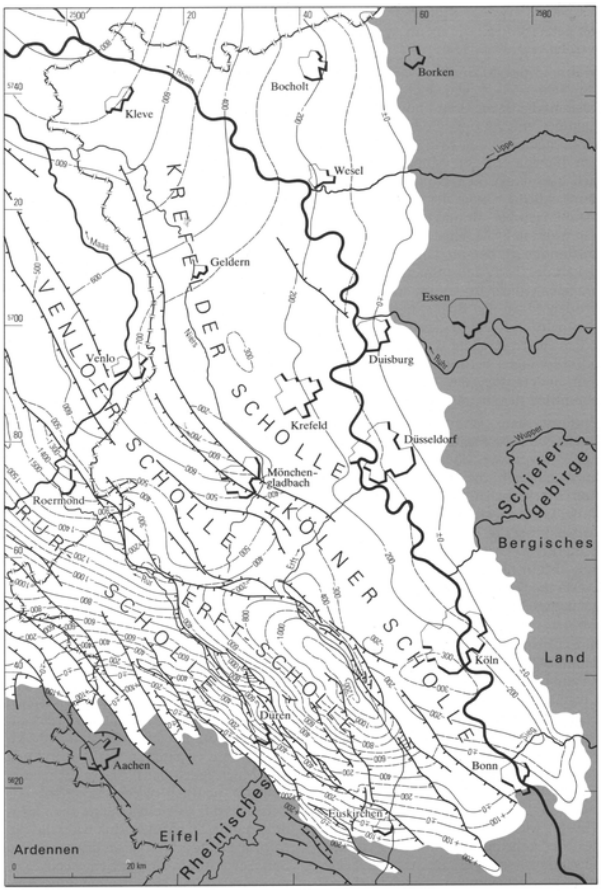

Fig. 2.1: Faults of the tertiary basement of the Lower Rhine Graben (white colored area; arrows: Rur-fault) and location of the open cast mine (circle). – Map width: 100 km (modified after GLA (1988)).

tribute to the shear zone, too, but to a much smaller portion (Figure 2.4). There is a wide range of literature on the problem of clay smear emplacement due to its great relevance to the assessment of fault permeability. Possible mechanisms are pointed out by Lehner and Pilaar (1997) based on outcrop data from open pits in Frechen, Germany, where the geological environment is very similar to that of this research. In this study, we will refrain from discussing mechanisms of clay smear emplacement and will focus on the structural aspects of shear zones that are related to fault roughness instead.

The deformation patterns in the fringe zone of a shear zone are dependent on lithology. Besides the continuous flexuring of layers, deformation is also supported by shear at dis-

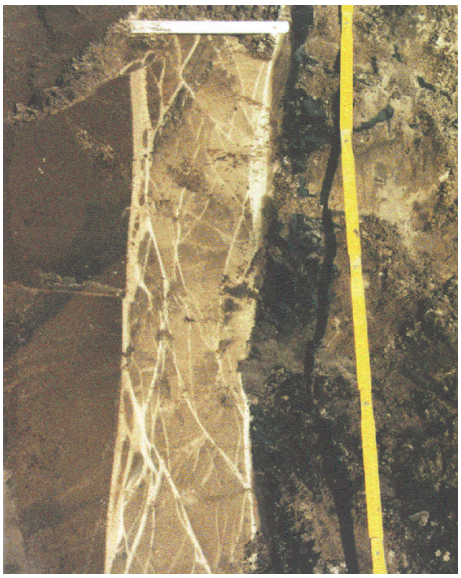

Fig. 2.2: Vertical section of a shear zone with sand displaced against lignite (left: sand, right: lignite; upper scale: 10 cm).

Fig. 2.3: Vertical section of a shear zone in lignite. – Fault walls are straight in general but show indentations of varying size filled with white clay smear (picture width: 2 m).

continuities. Common structures in sand are R-shears (Riedel-Shears) and the conjugated R'-shears that are known to appear in association with fault slip (Skempton 1966, Mandel et al. 1977, Mandl 1988, Logan et al. 1992). In lignite, the influence of faulting on rock damage gradually fades with distance from the shear zone (Figure 2.5). Fault parallel shears (so called D-shears) are usually found in distances up to several meters from the fault, whereas R-shears are restricted to the first meter and touch the fault gouge. Intense fragmentation of lignite appears at the immediate borders of the fault walls (Figure 2.6).

Fig. 2.4: Vertical cross section of a shear zone showing all lithologies that have been found in the fault gouges. Width: 25 cm. A: sand (footwall), B: lignite (hanging wall), C: clay layer, a: sand with bituminous clay (dark), b: dark clay and sand, c: white clay, d: bituminous clay, e: lignite fragments.

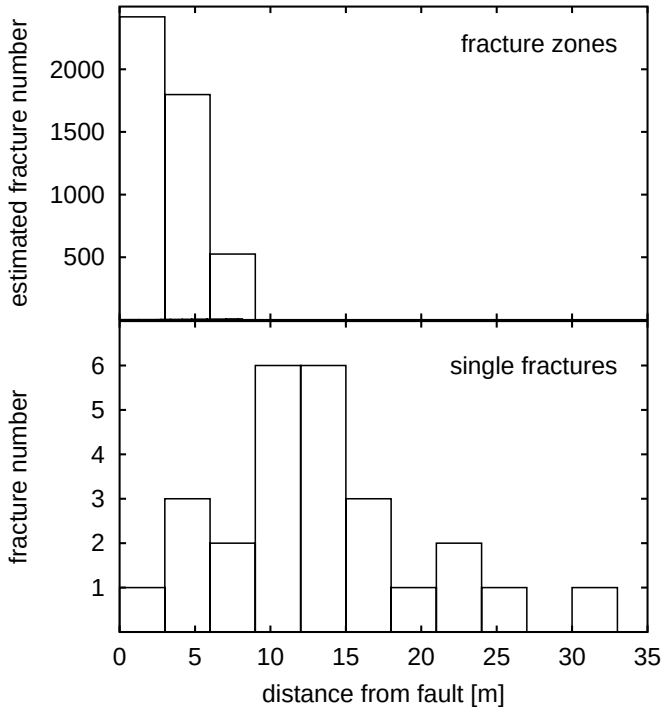

Fig. 2.5: Decay of fracture density in lignite on a scanline perpendicular to fault strike. – Fracture numbers for fracture zones estimated on the basis of the width and estimated fracture density of a zone.

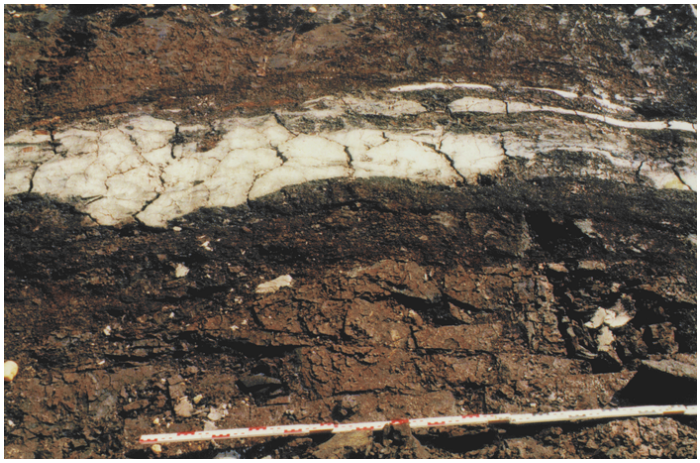

Fig. 2.6: Intense fragmentation of lignite adjacent to the clay smear (horizontal section; picture height: 1.24 m).

2.2 Data acquisition

In Hambach, mining activity has provided excellent fault exposures, especially in lignite. The exhaustion of the 50 m thick lignite seam ”Frimmersdorf (6C)” enabled the creation of large horizontal fault sections with the help of excavators. These unique exposure conditions allowed a detailed study of the roughness of shear zones in lignite at field scale. The main focus of this investigation therefore lies on structural phenomena in lignite. Additional fault observations were made in the overlying sand beds to examine the influence of lithology on structural phenomena related to fault roughness.

Three fault segments were selected within the major lignite seam to compare the structure of shear zones at different fault offsets. These sections also provide the data for the multi-scale analysis of fault roughness in the following chapter. The three fault outcrops are denoted with the literals A, B, and C, in the following. Outcrop lengths and fault offsets within the exposures are listed in Table 2.1. All exposures are located nearby, which minimizes the effect of varying geological conditions. The outcrop level of all faults is more than 3 m away from the top or bottom of the seam.

Large-scale structures were identified in mine maps and in the 330 m long exposure of fault A. Stratigraphy and fault offsets were extracted from borehole data, layer thickness data, and mine maps based on GPS-measurements of layer boundaries. Horizontal sections were created for joint measurement, and additional joint data in the environment of fault A

Tab. 2.1: Horizontal fault sections in lignite

outcrop ID	exposure length [m]	throw at exposure [m]
A	330	20 (SW) to 40 (NE)
B	20	10
C	60	4.5

and B was used with kind permission of S. Heidbüchel (see Figure 3.3).

The horizontal exposures A, B, and C provided high-resolution data sets of fault traces. The data was acquired by the following steps:

- *Fault preparation and photogrammetry.* The outcrops were leveled by an excavator and cleaned manually with a sharp spade to yield a clear boundary between fault gouge (mostly clay and lignite fragments) and host rock (lignite). Photographs of faults were taken from a lifting ramp or ladder and positioned relative to a local coordinate system with a positioning error of approximately 0.5 cm.

- *Postprocessing.* Fault traces were digitized with a sampling interval of 0.02 m (lifting ramp) and 0.01 m (ladder). The resulting data sets cover a scale range of 3 to over 4 orders of magnitude.

  Software tools were developed for the digitization of fault traces. They include programs for image rectification (shift objective), cutting, rotation, scaling, merging and segmentation using the German Gauß-Krüger coordinates. Digitization for the longest data set was performed in several steps:

  – Rotation and clipping of 28 pictures, each with a size of 200 MB to 300 MB to reduce the required memory size.

  – Automatic segmentation of the the fault gouge with manual correction of artificial disturbances.

  – Automatic digitization of fault traces.

  – Coalescence to a single data set for the foot wall and hanging wall, respectively (Figure 2.7).

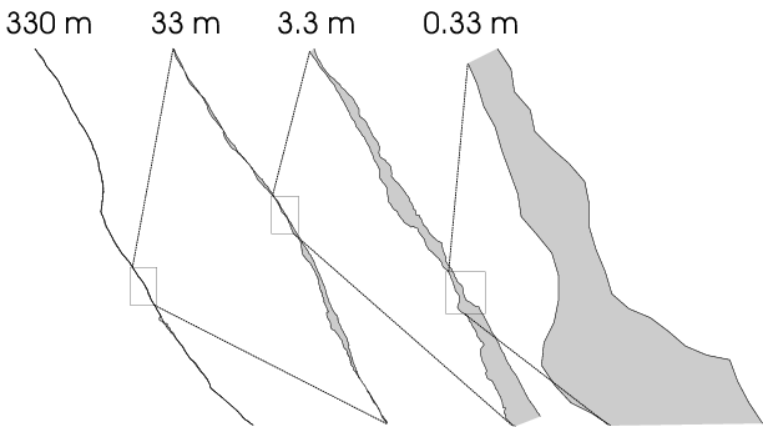

Fig. 2.7: Fault trace of the largest outcrop at different scales (fault A).

2.3 Reference surfaces for fault roughness

The idea of fault roughness needs a reference surface like, for example, a surface of maximum shear strain or shear dislocation. Shear strain concentrates on a delimited *shear zone* that can provide lateral borders as reference surfaces for roughness measurement. The difference between a shear surface and a shear zone is a matter of observation scale since every shear surface gains a three-dimensional structure if it is inspected from a smaller distance. Conversely, a shear zone turns into a shear surface if it is viewed from far away. However, the simple concept of a fault surface is not always supported by the natural phenomena. Strain must not always concentrate sharply with the result that neither a shear surface nor a shear zone can be identified at a given observation scale. In this case, the three-dimensional character of the fault cannot be neglected anymore. In the following, we will discuss possibilities of identifying reference surfaces in sand and lignite.

In sand, the fringe zone of a fault is subjected to substantial shear strain, which is supported by shear on subordinate shear surfaces. Due to the participation of secondary shears, surfaces of equal shear strain which could deal as reference surfaces are highly discontinuous and irregular. This means that, although shear deformation in sand is tightly coupled to localization, it is weakly concentrated, a fact, that inhibits a clear delimitation of a shear zone.

Faults in lignite usually show a sharp border between a cohesive host rock and a highly mobile fault gouge (Fig. 2.8). These borders provide good reference surfaces for roughness measurements. Only in few cases the damage of the fault walls is too intense to determine the extent of the fault gouge. Lignite fragments and large lignite splays are ascribed to the fault gouge if detachment from the host rock is obvious. The decision whether a rock body

is fully detached from the fault wall or not requires a three-dimensional view of the rock that is in fact not given. For this reason, the identification of the fault gouge cannot be totally free from subjective interpretation.

Fig. 2.8: Horizontal section of a fault gouge in lignite that solely contains white clay smear (picture width: 1.20 m).

Faults are usually observed in sections parallel or perpendicular to slip direction. The intersection of the reference surface with the exposure shall be called *fault trace* in the following. The roughness of the reference surface will be called *horizontal* and *vertical roughness* depending on whether it refers to a horizontal or vertical section. Since the entire work deals with normal faults, the first term denotes the roughness perpendicular to slip direction, whereas the second refers to the roughness parallel to slip direction.

Chapter 3

Field observations

3.1 Characteristics of fault roughness

3.1.1 Segmentation

A fault surface can contain isolated segments reflecting a self-contained structural evolution of this part of the fault. Segmentation can develop, for example, by coalescence of fractures to a continuous fracture zone or by intermittent phases of fault propagation. Segmentation provides the source for an identification of processes responsible for fault roughness.

In general, a rough fault surface does not need to be segmented. A segment is characterized by a specific structural property that holds out over a certain interval of the fault surface and then breaks off rapidly. This can be, for example, a linear or arcuate trend that suddenly leads over into an unstructured rough fault surface. A clear lateral termination of the specific property is necessary for delimitation and thus for identification of segments. If delimitation is problematical, segments will be difficult to identify even if there is a distinct fault roughness. This is a crucial point in the analysis of fault segmentation complicating the extraction of structural processes from the fault trace. Additional field data and mechanical arguments shall therefore be used to confirm the plausibility of the findings.

3.1.2 Incorporated joints

Joints are typically planar on the scale of the entire structure, which attributed to the ability of mode-I cracks to propagate in plane. Linear segments similar to joints can be found in horizontal section ”A” at several locations (Figure 3.2). Linear segments are absent in sand, probably because the only slightly consolidated sand beds are unaffected by jointing. The interpretation of linear segments as incorporated joints is not univocal. Linear segments in

lignite enclosing high angles to the local fault strike could also be R-shears due to contemporaneous strike slip movements of the fault. However, the observed segment orientations would not indicate a uniform strike slip direction, so that incorporation of joints by a propagating fault appears to be the more reasonable.

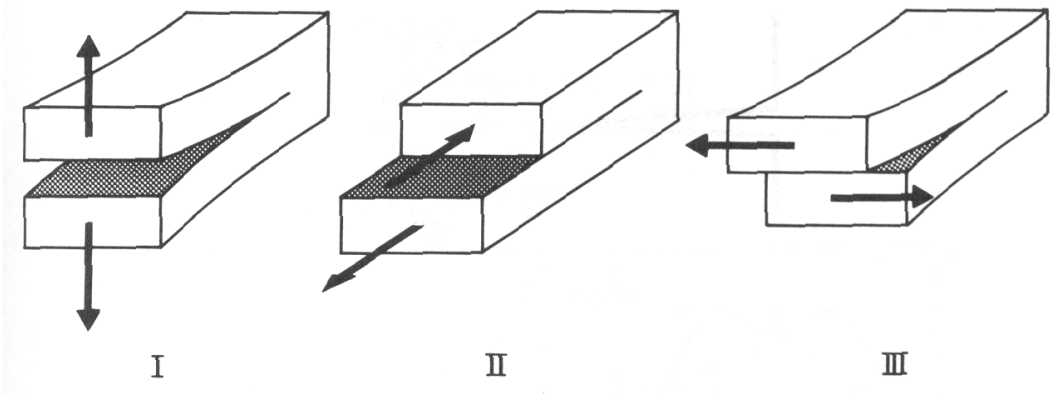

Fig. 3.1: Crack modes I, II, and III (from Scholz (1990)).

This interpretation is underlined by the fact that incorporation of joints by fault growth will take place within the lignite seam if the fault system is reactivated. Figure 3.3 (page 28) illustrates the recent situation, showing joints with lengths greater than 10 m in the environment of three faults. Apparently, joints are oriented almost parallel to the faults except for the zone of fault overlap, called *relay zone*. Here, a subsidence of the common fault block cannot be maintained by fault slip, which is indicated by the decrease of the total fault offset at the zones of fault overlap (Figure 3.4, page 28). The missing offset has to be compensated by deformation of the relay zone, which leads to the observed scatter of joint orientations. In case of further extensional tectonic activity the faults will grow and probably merge under formation of an eye structure. The faults will be forced to propagate through the disturbed joint system, thereby incorporating joints with high angles to the fault strike.

It shall be noted that Figure 3.3 also illustrates the coupling of different structure scales which is essential for fault complexity. The interference of faults at relay zones takes place on a large scale but influences the evolution of joints at a very much smaller scale. If these joints are incorporated by the propagating faults they are able to influence fault roughness and lastly the large-scale behavior of the fault system. This example of scale coupling clearly illustrates again the complexity of the observed fault system.

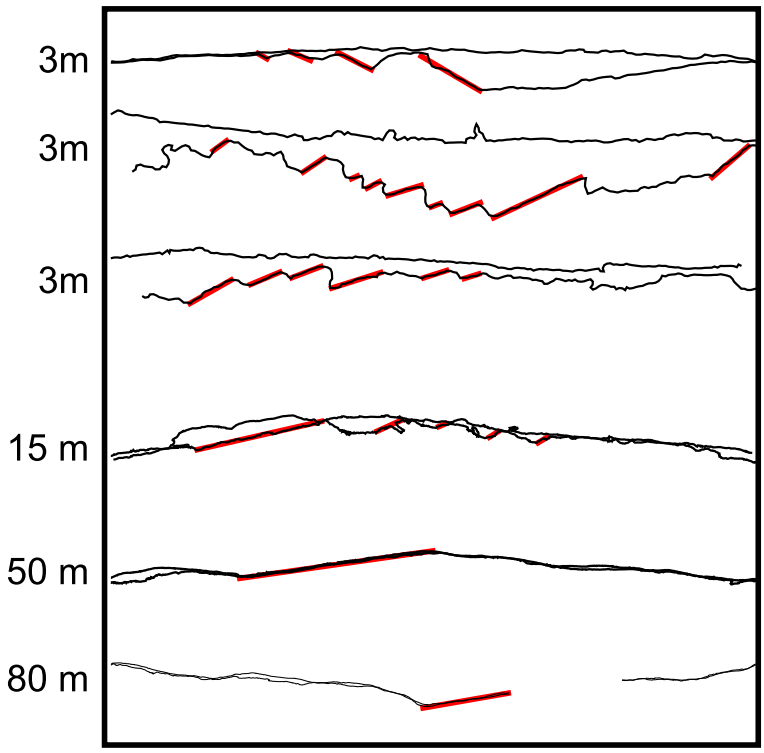

Fig. 3.2: Linear fault segments in lignite, probably referring to incorporated joints.

3.1.3 Arcuate segments

A large arcuate segment was found in lignite (Figure 3.5). The structure ends at one side with a sharp kink of the fault trace but is not well limited on the other. The extent of arcuate curvature can therefore only be roughly estimated to 50 m in length and 5 m in width. Horizontal sections in sand do not show any arcuate segmentation. Although fault traces in sand are undulated, arcuate curvature does not occur in form of self-contained segments with a sharp delimitation at one or two sides.

As far as the horizontal growth of a normal fault corresponds to mode-III cracking the lateral propagation of the fault should be linear. There are several reasons why a fault might choose an arcuate growth instead. The mergence of two sub-faults that are not arranged in a plane, for example, can only be achieved by a curved fault propagation. Mandl (1988) has proposed two alternative mechanisms for arcuate fault growth. Firstly, the bending of a fault wall reduces the normal stresses in direction of the fault strike (Figure 3.6). Since both fault walls usually do not suffer the same amount of flexuring, the principle stresses at the fault

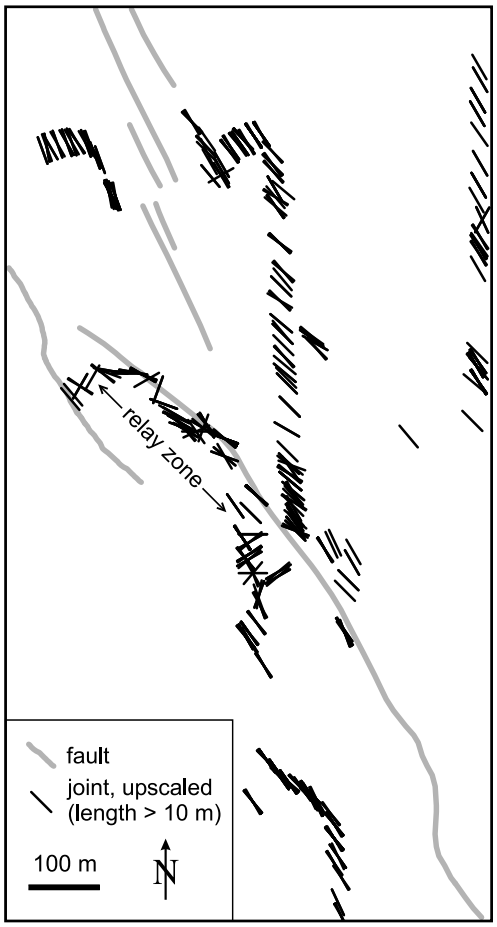

Fig. 3.3: Map of fault system and joints with length over 10 m.

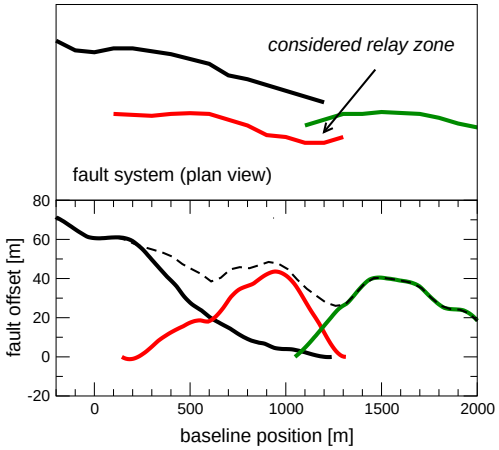

Fig. 3.4: Distribution of fault offsets along the fault profiles.

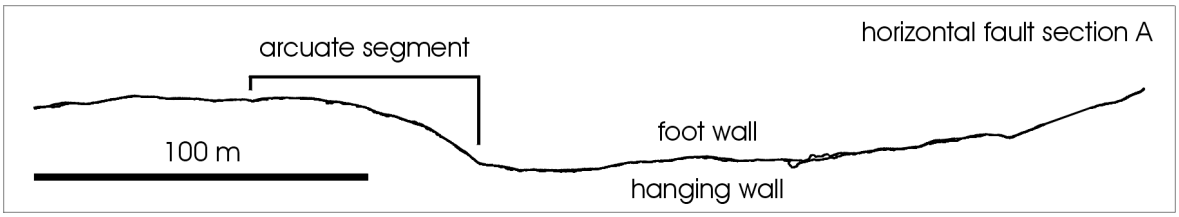

Fig. 3.5: Large arcuate segment in the horizontal section A (lower fault block is hanging wall).

tips are rotated. This forces the fault to grow in direction of the fault block with the strongest bending. Secondly, the direction of fault growth can be influenced by shear softening of the fault. Shear softening of an inclined fault relieves the foot wall and in turn adds additional normal stresses on the hanging wall in direction of the fault dip. Consequently, the critical stress state for fracturing will be reached earlier on the down-thrown block attracting fault propagation towards the hanging wall.

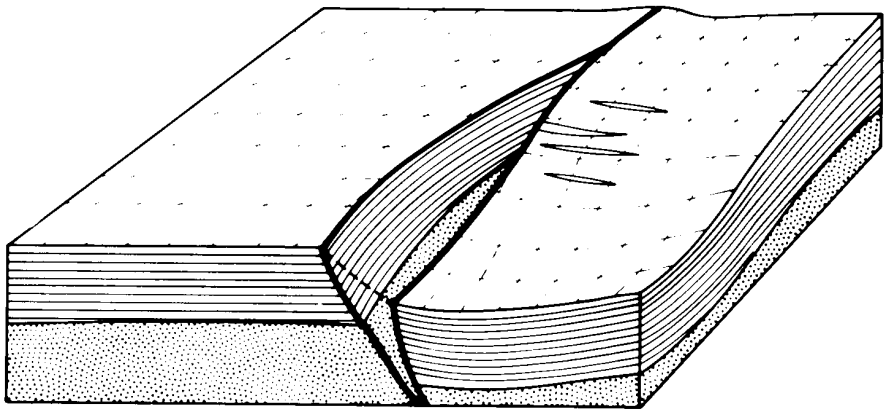

Fig. 3.6: Bending of the down-thrown block causes extension, indicated by extensional fractures (Mandl 1988).

3.1.4 Vertical roughness

Vertical exposures of shear zones in lignite as well as in sand are very straight at the 1 m to 10 m scale. In lignite, vertical roughness is restricted to decimeter-wide indentation in the fault walls, which are no hindrance for a slipping movement (Figure 3.7). A high variability of vertical roughness at small scale is indicated by the fault dip, measured every 4 m along the fault trace of section A (Figure 3.8). The variation of dip angles is probably attributed to indention structures.

Comparing horizontal and vertical roughness in lignite shows a strong anisotropy of fault roughness. This anisotropy is reasonable from a kinematic point of view since horizontal roughness does not inhibit slip and thus has more freedom to develop and persist during fault displacement. On the contrary, vertical roughness is subjected to friction and wear. Even if the initial fault propagation in slip direction might be rough, lastly only those fracture patterns will participate in the formation of the main shear zone that are smooth enough to allow fault slip.

Investigation of vertical roughness at large scales is obstructed by the size of vertical fault sections, which is usually limited to heights below 20 m. Vertical roughness at larger scales has to be assessed by comparing true and apparent dip angles (Figure 3.8). For so called *cylindrical faults*, which per definition have no roughness in slip direction, the apparent dip angles measured in slip direction, i.e. approximately perpendicular to the *global* strike, are constant. If the fault has no vertical roughness, true dip angles, measured perpendicular to the *local* strike, are increased against the apparent dip angles. This is indeed the fact at the large arcuate segment in the middle of exposure A (Figure 3.8). Here, the true dip angles are raised in order to maintain constant apparent dip angles, i.e. a cylindrical fault geometry. This shows that horizontal fault roughness does not necessarily indicate a vertical roughness. However, the dip measurement contains some noise due to indentation structures, which obstructs an identification of vertical roughness at large scale.

The fault roughness displayed in Figure 3.5, and especially the large arcuate segment, raises the question whether the fault is able to maintain this topography in vertical direction over the entire fault surface that crosses several lithologies. It seems reasonable that this cannot be the case. If horizontal fault topography should change in dip direction this will

Fig. 3.7: Vertical section of a fault in lignite showing indentations at the decimeter scale (picture width: 2 m).

most likely happen at the boundaries of layers with different mechanical properties. It was mentioned previously that arcuate and linear segments present in lignite are absent in sand layers, where roughness is much smoother. Thus, steps and jogs of the fault surfaces can be expected in the transition of sand and lignite. The occurrence of a large splay fault in exposure A approximately originating at the bottom of the lignite seam (see Figure 3.9 and discussion below) underlines that layer boundaries are a likely primary source for vertical roughness giving rise to compressional or extensional structures.

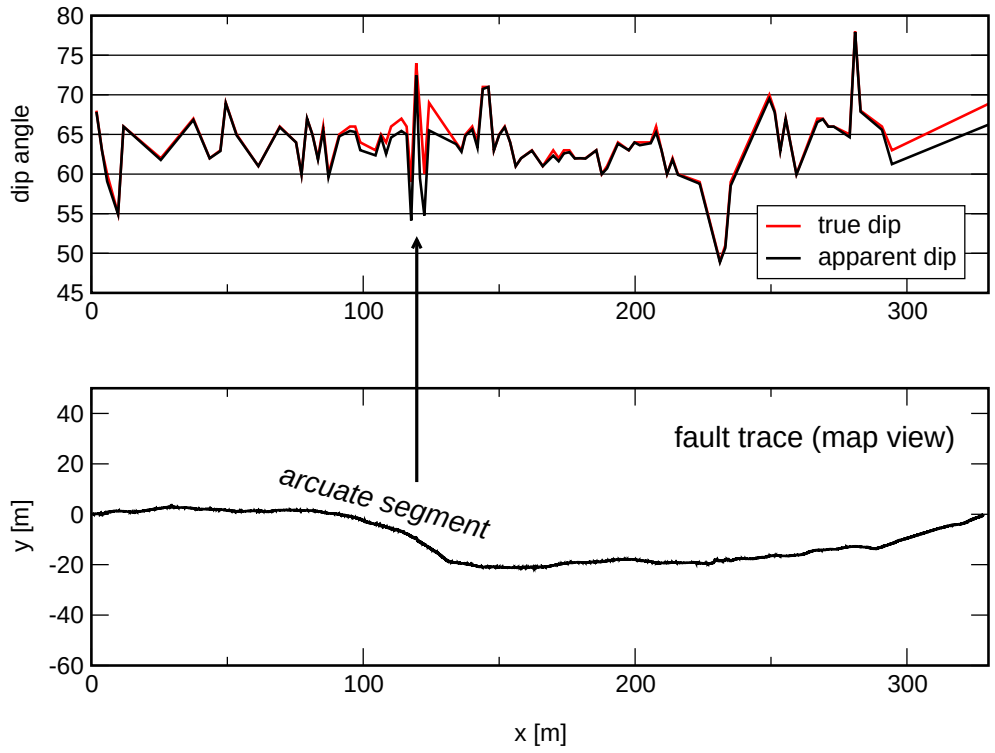

Fig. 3.8: True and apparent dip angles for the evaluation of fault cylindricity.

3.2 Damage phenomena induced by fault roughness

3.2.1 Large splay faults and associated damage

Faults in lignite and sand are frequently accompanied by *splay faults* reaching lengths of several 100 m (measured in strike direction), thereby traversing sand and lignite layers (Figure 3.9 top). Splay faults are usually found on the hanging wall of a fault forming wedge shaped bodies of rock (Figure 3.9 bottom). Large splay faults carry significant fault offset. In horizontal section A, the offset varies between 5 m and 10 m which is about 15 to 30 % of the main fault's offset.

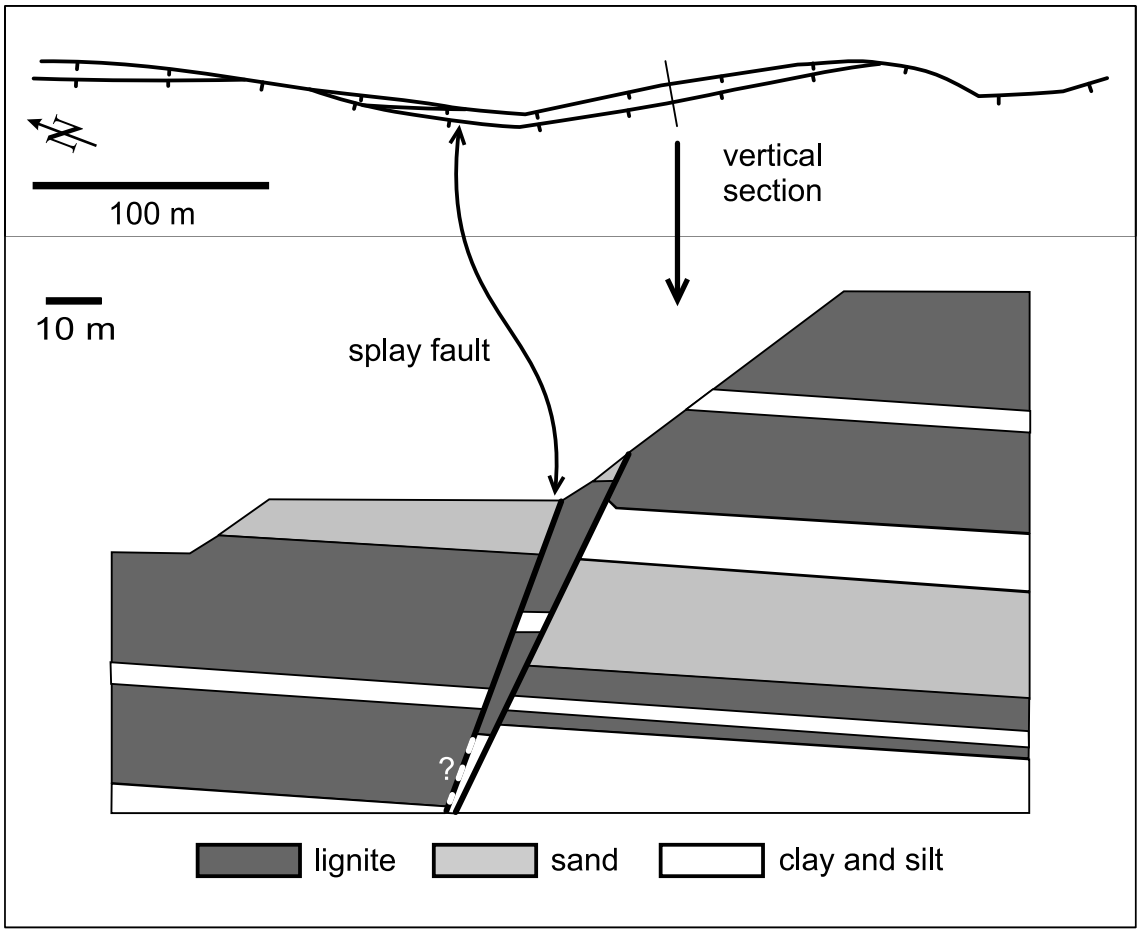

Fig. 3.9: Horizontal and vertical section of the splay fault of exposure A. – The branching position of the splay fault in the vertical section is linearly extrapolated by means of dip measurements and need not reflect the real situation.

Large splay faults are accompanied by fault wall damage on a broad scale range. The splay, i.e. the rock between splay fault and main fault, suffers increased deformation. Damage is strongest in the horizontal and vertical branching zones of both faults. Horse structures and complicated fracture patterns have been found here in lignite (Figure 3.10).

Splay faults can evolve prior to the main shear zone. Patton et al. (1998) have shown in experiments with limestone plates that evolving shear cracks can switch their propagation path to the direction of precursory mode-I microcracks (Figure 3.11). Since these fault segments do not sustain the shear strain of the plate they are in-activated during fault displacement. However, this process was only noticed at high confining pressures (200 MPa) in the experiment. Since all considered faults were formed at shallow depths, a development of splay faults prior to the main shear zone is unlikely.

According to the vertical section in Figure 3.9, the large splay fault of exposure A approximately initiates at the bottom of the lignite seam. This might indicate that the splay fault was formed due to a fault step at the lithological boundary of sand and lignite. In this case, the splay fault can be explained as R-shear above a zone of increased friction (Figure 3.12): the subsidence of the hanging wall over the interlocked fault segment induces a shear strain parallel to the fault forcing the maximum principle stress axis to rotate. The shear fracture evolving in this local stress field according to the Mohr-Coulomb fracture criterion is an R-shear.

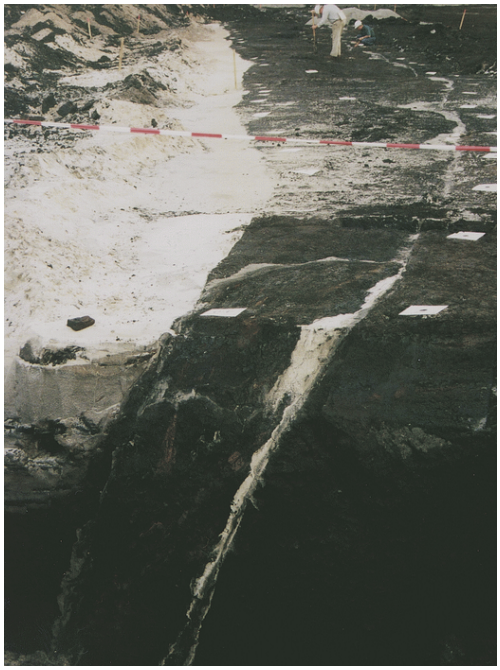

Fig. 3.10: Horse structure at the branching zone of main fault (white shear band to the right) and splay fault (shear band between white sand and dark lignite to the left). – Lower part of the picture is a vertical section; upper part is a horizontal section. Picture width: approx. 3.5 m

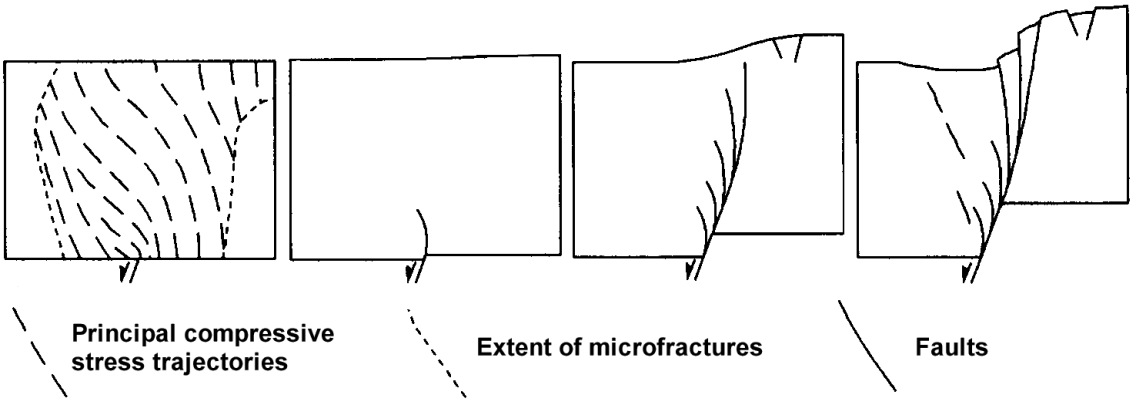

Fig. 3.11: Fault generation in a 1 cm thick limestone layer at 200 MPa confining pressure (after Patton et al. (1998)). The splay faults form as primary structures here.

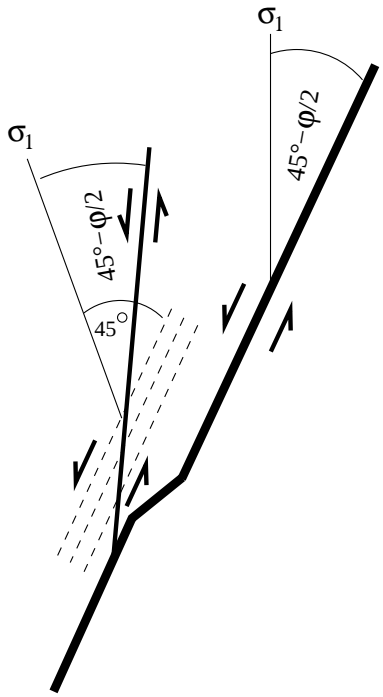

Fig. 3.12: Generation of an R-shear at a fault step (σ_1: maximum principle stress, ϕ: internal friction angle). – The subsidence of the hanging wall imposes a shear strain parallel to the fault plane (stippled lines). This is equivalent to a local rotation of the maximum principle stress axis. A Mohr-Coulomb fracture relative to this stress field is an R-shear.

3.2.2 Fault wall damage at the m-scale

Damage zones

Fault walls frequently display strong damage. In lignite, there are bands of intensely fragmented rock (Figure 3.13), whereas bleached shear bands appear in sand (Figure 3.14). The intensity of damage varies along the fault and penetrates the fault wall into depths of several decimeter. In exposure A, which shows the highest offsets of all sections (30 m), damage is stronger on the hanging wall. Possible reasons for this asymmetry are discussed in section 3.2.2.

Fig. 3.13: Horizontal section showing damaged lignite adjacent to the white clay smear (left side is foot wall).

Fig. 3.14: Horizontal section showing bleached white shear surfaces in sand at the contact to lignite (left side is foot wall).

Fault wall damage indicates stress concentration at restricted parts of the fault indicating raised friction. High friction requires high friction coefficients that can only be obtained by local interlocking of asperities. From a kinematic point of view, damage of asperities allows maintenance of fault slip. It was commonly observed that the intensity of damage did not

fade gradually with distance from the fault but dropped off rapidly after a few decimeters due to preexisting fractures or shear bands that detained further propagation of damage into the fault wall.

Splay faults and splay fractures

In lignite, zones of fragmentation are often limited by splay fractures with a horizontal width of 1 m to 10 m measured in strike direction (Figure 3.16). These fractures show no apparent shear offset due to the absence of markers. In sand, deformation and damage of fault walls is typically associated to splay faults which are similar to the splay fractures in lignite but show a clear shear offset (Figure 3.17). Flexuring due to fault slip is supported by splay faulting and takes an important part in the formation of the fault gouge (Figure 3.15). This explains the irregular shape of many shear zones in sand.

The inclination of 20° to 30° to the main fault as well as the shear sense suggest that splay faults are R-shears. The situation is less clear for lignite since the fractures cannot definitely be identified as shear fractures.

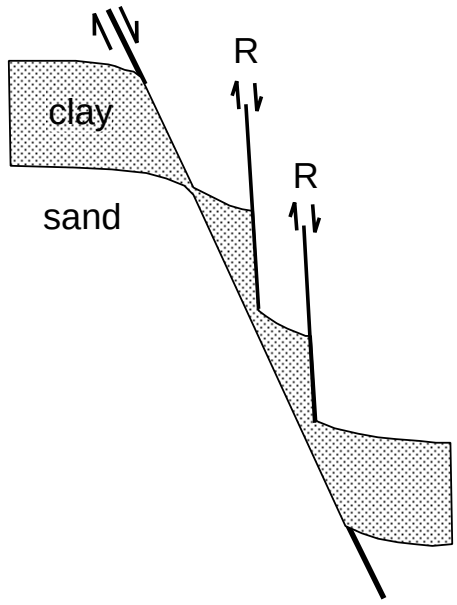

Fig. 3.15: R-shears creating clay ”parcels” and forming a fault gouge with irregular thickness. Note that only a small part of the clay parcels support fault slip in this early stage of faulting. In the course of fault offset, parcels are flattened by simple shear and incorporated into the shear zone.

In general, R-shears can evolve before as well as after the formation of the main shear zone. Lehner and Pilaar (1997) have described similar structures in sand formed prior to the main fault by a flexuring of the strata (Figure 3.18). R-shears associated to the flexure are

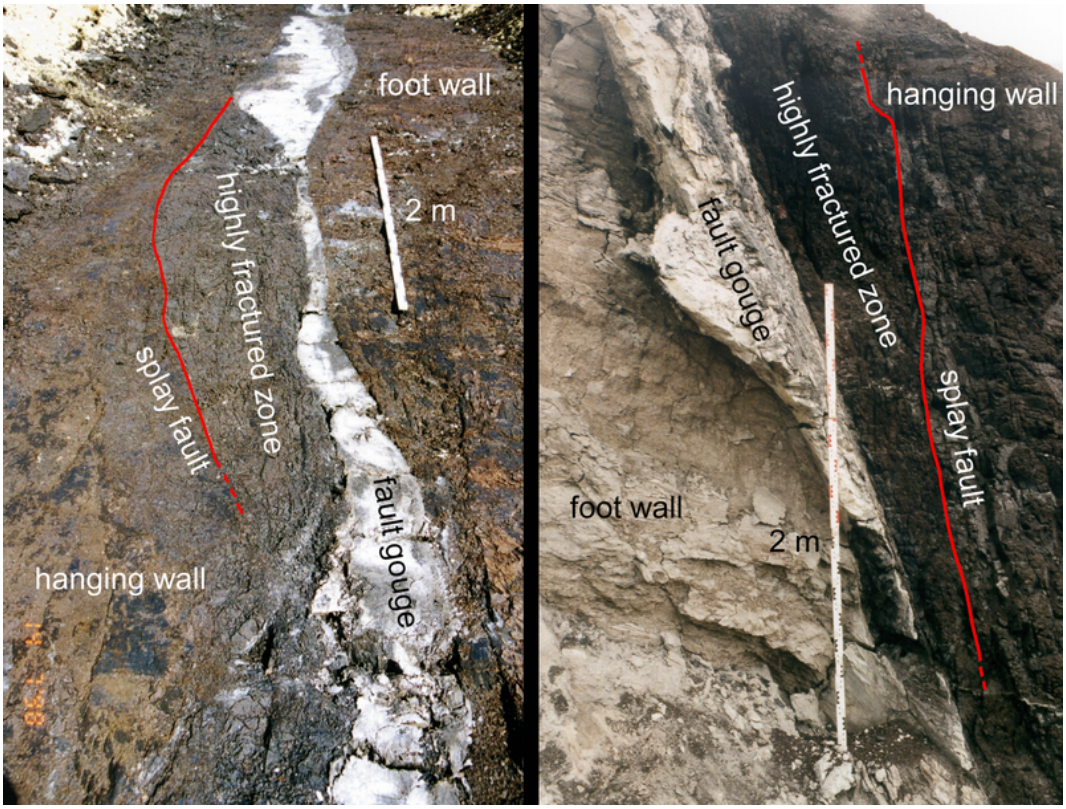

Fig. 3.16: Typical damage structures in lignite related to splay faults. Left: oblique view on horizontal section. Right: vertical section with sand on foot wall.

cut by the evolving main fault and afterwards dislocated by the fault offset. Characteristical for this process is that the offset of the R-shears suddenly terminates at the intersection with the main fault, indicating a secondary formation of the main shear zone. Yet, most of the observed splay faults in sand do not show this behavior and their offset contributes to the offset of the main shear zone. The process proposed by Lehner and Pilaar (1997) can also not explain the splay fractures found in lignite because the necessary flexuring of the lignite seam is missing.

It can be noticed in horizontal sections in sand and lignite that lateral parts of splay fractures change orientation and merge with the main fault. This indicates that at least these lateral parts are younger than the main shear zone. Consequently, the observed splay faults cannot be entirely of primary origin.

Additionally, the association of splay faulting with the intense damage of the fault walls suggests that both structural features have evolved due to the same mechanism. Heteroge-

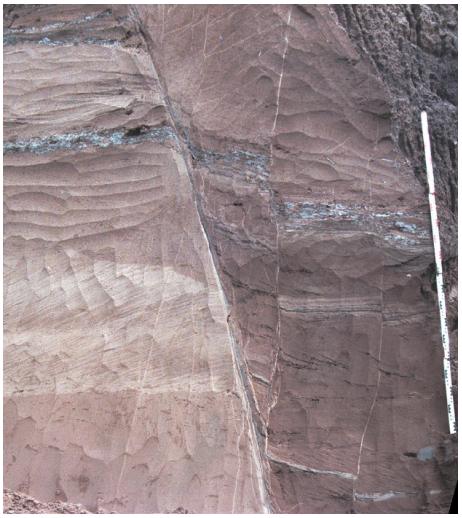

Fig. 3.17: Splay faults in sand.

neous friction along a rough fault provides a reasonable explanation: If slip is inhibited by interlocked asperities, the subsidence of the fault block above the pinned fault section induces a shear strain parallel to the fault surface (Fig. 3.12, page 34). The shear strain forces the maximum principle stress axis to rotate until it reaches an angle of 45° to the normal vector of the fault. The fault block pushes from one side at the interlocked segment and pulls from the other. Consequently, the differential stresses will grow until either slip or failure will occur. In the latter case, the evolving Mohr-Coulomb failure will be located at the pulling part. However, this splay fracture still does not enable slip. Since lignite shows brittle behavior, the interlocked asperities can only be overridden by damage and wear (Figure 3.19). The extent of damage is limited by the precursory splay fracture, which is acting as a mechanical barrier. In this way, friction at rough faults can explain splay fracturing as well as the associated damage of the splays. The process is not bound to a contiguous separation of the fault blocks so that it might already have taken place at the very beginning of fault evolution.

If the observed faults are rough in slip direction, which is suggested by the field observations, damage and wear should be a secondary process that still accompanies fault activity. Yet, parts of the splay faults might be older than the main shear zone. Since splay fractures grow from the fault plane into the relic process zone of a fault, they may have incorporated some of its fractures. Frequency and orientation of splay fractures might therefore reflect properties of the process zone.

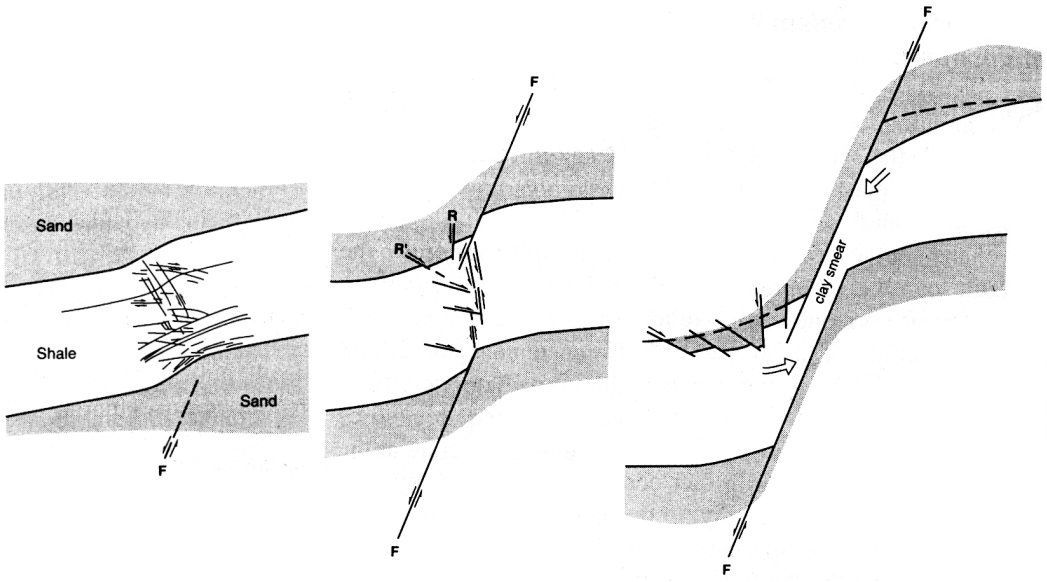

Fig. 3.18: Splay faults formed by flexure of a shale bed (Lehner and Pilaar 1997).

Detachment of fragmented lignite

In horizontal section A, lignite fragments of varying size covered 8% of the fault gouge area. The field observations support that lignite fragments are detached from zones of intense fault wall damage and spread into the fault gouge (Figure 3.20).

Considering the fault thickness of section A, one finds that detachment of lignite is important for the alteration of fault surfaces. Fault thickness will be calculated as the distance between foot and hanging wall traces perpendicular to a straight global baseline that runs through the mean start and end point of both fault traces (if a definite determination of the thickness-function at a certain position is inhibited by a high tortuosity of the profile, the maximum thickness is chosen; interpolated sections of the fault traces were not regarded in the measurement). A fault with negligible offset should have a negligible fault thickness since both fault walls match to each other perfectly. In section A, the mean fault thickness amounts to 23 cm (Figure 3.21). Since most of the fault gouge consists of clay (only 8% is lignite), this indicates a considerable misfit of the fault walls and an increase of fault gouge volume. The mechanism of creating additional fault gouge volume cannot have been a simple separation of fault blocks because foot and hanging wall are in contact in all exposures (Figure 3.21 shows a high frequency at the smallest thickness bin). There are two ways of increasing the fault gouge volume under continuous contact of the fault blocks. In case of fault surfaces with high and permanent roughness, fault blocks can be forced to separate due

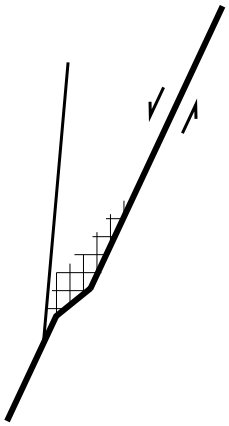

Fig. 3.19: Location of damage needed to override interlocked asperities.

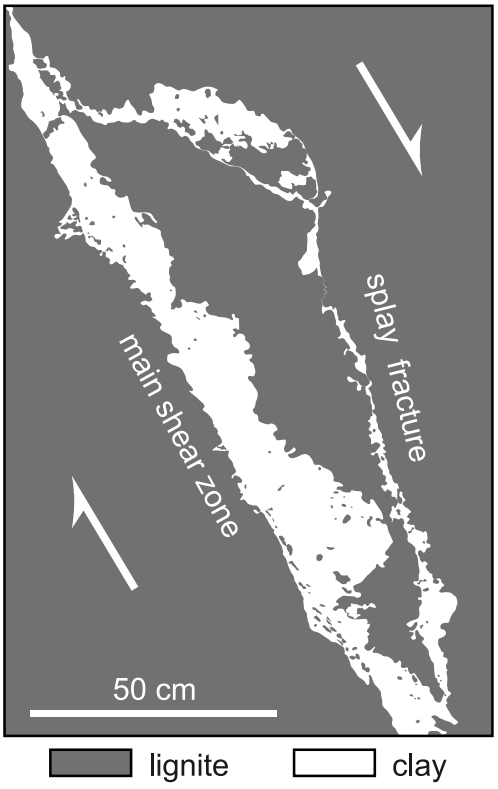

Fig. 3.20: Vertical section of the main shear zone (section A) showing detachment of damaged lignite from the hanging wall.

to an increasing mismatch at ever larger scales. If, on the other hand, roughness amplitudes are low, volume can only grow by an outflow of detached host rock out of the fault zone and into the top or bottom layers. The straightness of fault traces observed in vertical profiles objects against fault wall separation due to high roughness amplitudes and therefore indicates that detachment of lignite and transport into the adjacent layers is the main reason for the observed increase of clay volume within the fault gouge.

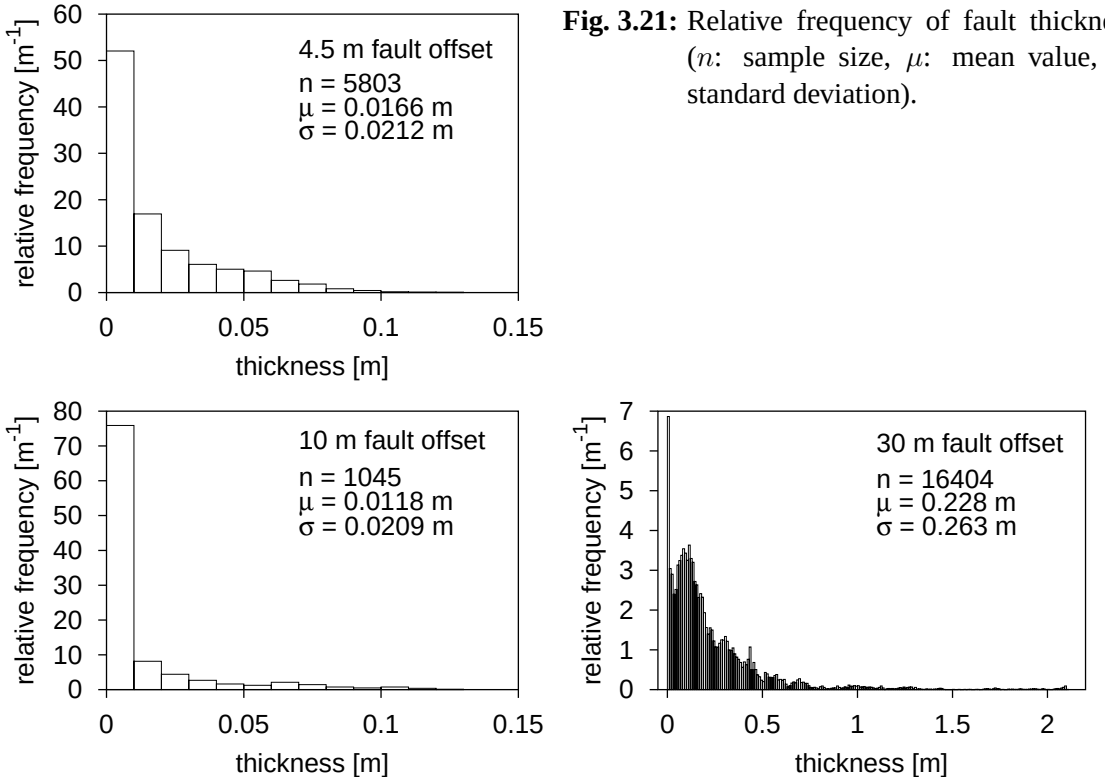

Fig. 3.21: Relative frequency of fault thickness (n: sample size, μ: mean value, σ: standard deviation).

Reasons for asymmetry

Fault roughness is modified by detachment of lignite fragments from damage zones. Thus, the asymmetry of damage noticed in lignite, be it with or without splay faulting, will be of importance for the multi-scale analysis of roughness in the following chapter. Several possibilities of how asymmetrical damage can evolve shall be discussed in the following; some are of mechanical nature, some are bound to the geometrical aspects of the exposure relative to the tectonic situation.

- The asymmetry of damage may reflect the asymmetrical stress conditions at a propagating fault tip. Usually, the density of mode-I fractures is higher on the dilatational side of a fault leaving behind an unequal strength of the rock (Scholz et al. 1993, Mandl 2000).

  Since mode-I cracks have an oblique orientation to the fault – which is a mode-II fracture – there is also a mechanical anisotropy of the process zone that prefers splay faulting on the hanging wall (Moore and Lockner 1995, Patton et al. 1998, Willemse and Pollard 1998).

- Normal faults usually show a higher mobility of the hanging wall due to the different shape of the fault blocks. The higher deformation adds additional stresses to the down-thrown block which favors asymmetrical damage (Mandl 1988).

- Mandl (1988) points out that the reduction of shear stresses due to shear softening is compensated by increasing the normal stress on the hanging wall in direction of the dip vector. This implies that the Mohr-Coulomb fracture criterion is reached earlier on the down-thrown block.

- Stability of the fault walls is decreased at top and bottom of the lignite seam. Since the outcrop level comes closer to the seam borders on the hanging wall, this side should show higher damage in the outcrop (Figure 3.22).

- Clay smear lowers the friction coefficient and protects the fault walls from damage. In the outcrop level, the total amount of offset over which fault walls were lubricated by clay smear is higher for the foot wall (Figure 3.23). This may cause higher damage on the hanging wall.

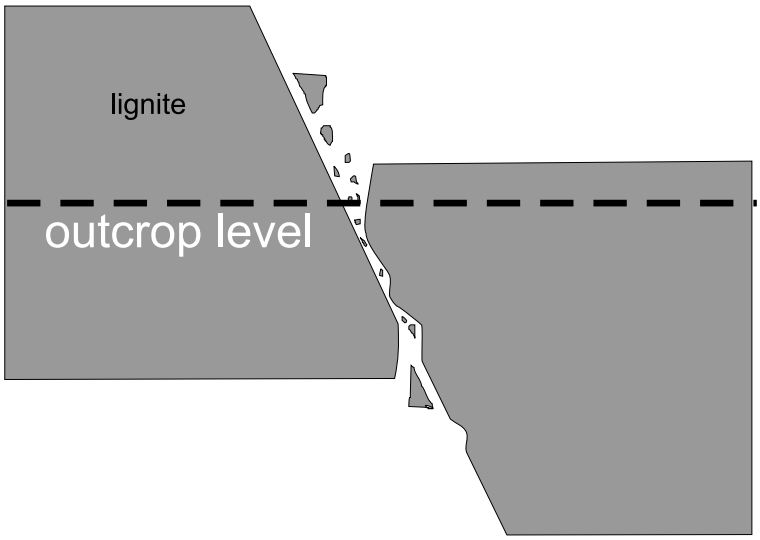

Fig. 3.22: Apparent asymmetry of damage due to reduced seam stability at the seam top and bottom.

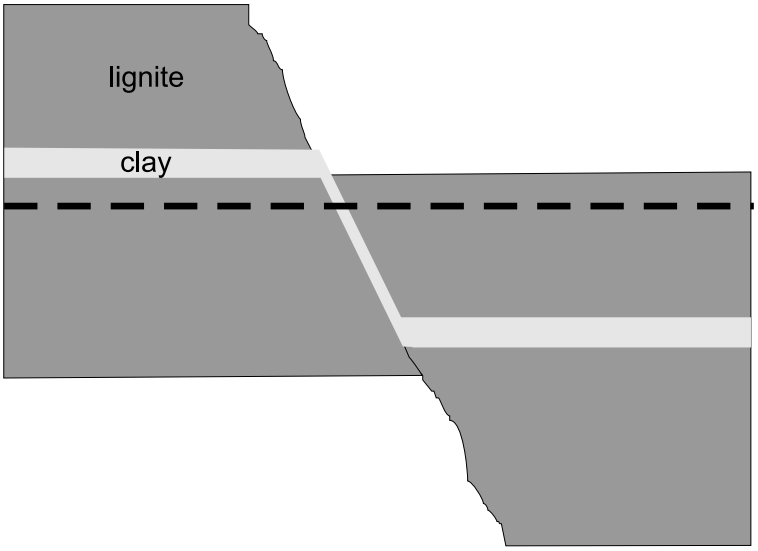

Fig. 3.23: Apparent asymmetry of damage due to different lubrication time.

3.3 Discussion

We find that the rough topography of the investigated faults still exhibit evidence for segmentation owing to the process of fault formation. Arcuate fracture growth and incorporation of planar fractures provide a reasonable explanation for the arcuate and linear fault segments found in exposure A. The large splay fault of exposure A suggests that there is a fault jog at the bottom of the lignite seam pointing out that material heterogeneity contributes to the formation of fault roughness. The indentations of the fault walls found at scales below 10 m are late segmentation structures. Since they are caused by detachment of damaged lignite they are bound to frictional fault slip rather than to fault nucleation.

According to the observations, fault formation is a process that changes its characteristics but does not come to rest as long as slip takes place. The first stage of fault formation is governed by coalescence of fractures and non-planar fault propagation. Material heterogeneities seem to play an important role for the creation of vertical roughness. The second stage begins as soon as roughness takes over an active part in structure formation due to fault slip. Friction between rough fault walls produces splay faults and fragmentation zones and triggers the previously mentioned processes of fracture coalescence and non-planar fracture propagation at scales well below the fault size. Thus, fault roughness introduces an additional process of scale coupling in the sense that a large structure (the fault) influences pattern formation on sub-scales (damage zones). Since roughness stems from the mechanical interaction of structures on these sub-scales, scale feedback is introduced. Thus, roughness influences the way how faulting organizes multi-scale patterns.

Chapter 4

Multi-scale analysis of fault traces

4.1 Measuring roughness

Scale-dependent measures used to analyze fracture roughness (Klinkenberg 1994, Develi and Babadagli 1998) can be classified into isotropic and anisotropic measures according to their dependency on the orientation of a fracture profile. Each type reflects a different concept of roughness which is more or less adequate for the description of natural fractures.

In literature, anisotropic measures are used to quantify the fractal scaling of faults and fractures. Usually they are derived from the perpendicular deviation of the fracture trace from a straight baseline providing profile heights $h(x)$ as a function of profile position x. This requires a not too tortuous fault trace to ensure a well defined, i.e. single-valued function. According to such a measure, fractures often show self-affine, i.e. an anisotropic fractal scaling. A fracture profile $h(x)$ is self-affine if it is statistically equivalent to the rescaled profile $r^H h(x/r)$, where $r > 0$ denotes the scaling factor for the x-axis and r^H the one for the h-axis. H is called the Hurst (or Hausdorff) exponent and determines the scaling relation between the x- and h-axis. For $0 \leq H < 1$, the one-dimensional profile function is fractal and has a fractal dimension of $D = 2 - H$ (Feder 1988). The function gets smoother for H moving from 0 to 1. For $H = 1$ the function is "self-similar" because both axes scale in the same way, but the function is not fractal any more.

Measuring roughness in only one direction is based on the assumption that the processes which are responsible for fault roughness act perpendicular to a straight global baseline. The widespread use of baseline-derived measures for the fractal analysis of fractures and faults proves this approximates the natural phenomena quite well. Although roughness of natural fault traces is anisotropic, however, the direction of anisotropy is not homogeneous. This may prove problematic if the considered scale range is too large. Since the tortuosity of fault

traces increases with decreasing scale the requirement of a single-valued function may not be satisfied anymore if too small scales are take into account. The heterogeneity of scaling direction might refer to the fact that the orientation of local stress fields may differ strongly from that of the global stress field acting on the fault.

Usually it is difficult to find out why roughness scales in a specific way. If the influence of a certain fault structure on scaling shall be assessed this structure type should produce or inhibit a significant amount of roughness at a certain scale range. According to a baseline-derived measure the roughness amplitude does not only depend on the type of the structure but also on its orientation. Linear segments caused by joints, for example, will provide different roughness for different inclinations to the global baseline. A structural interpretation of roughness by means of a baseline-derived measure is therefore only possible if the structures of the considered type show similar orientation. Another problem is that a tortuous fault trace can produce significant noise. A linear fault segment, for instance, with a high angle to the global fault strike has very strong high frequency components which may cloud the roughness of small structures even if this structure occurs only once on the fault trace.

The mentioned problems are bound to the the assumption of a straight baseline and are not an inherent property of anisotropic measures. Anisotropic measures which are better adapted to natural faults require a location and scale dependent baseline. This can be achieved by the classical measures *root mean square roughness* (RMS), *average roughness* or *maximum-minimum difference* if profiles are detrended for each considered scale (Develi and Babadagli 1998, Malinverno 1999). An alternative solution are *isotropic roughness measures*, which are usually applied to the curve of the fracture trace and are completely independent from the orientation of the profile. The classical *divider* or *ruler method* is a well known example. Isotropic measures are able to deal with highly tortuous fault traces and provide constant roughness amplitudes for a certain structure type independent of its orientation.

Still, anisotropic measures which refer to a global baseline are needed for fractal analysis. One can readily see that isotropic measures are not able to quantify self-affine, i.e. anisotropic scaling laws. Anisotropic measures referring to local baselines are used in literature for fractal analysis, too, but they actually are less suited for this purpose because their behavior cannot be predicted by the theory of fractional Brownian motion any more. In this study, an anisotropic measure will be used for fractal analysis whereas an isotropic measure will be applied to identify processes that create characteristic scales of roughness.

4.2 Fractal analysis

4.2.1 Method

For fractal analysis the fault curves were transformed to a discrete height function $h_i \stackrel{\text{def}}{=} h(x_i)$. Heights were measured perpendicular to a global baseline running through the mean start and ending points of the adjacent fault traces. The tortuous fault trace of exposure A locally provided more than one height value at some profile positions. At these locations those height values were chosen which produced the maximum fault gouge thickness. An identification of the fault trace failed at some locations of exposure A, partly due to a 14 m wide road crossing the outcrop. Missing intervals like those were linearly interpolated. The artificial fault topology introduced by this proceeding will be regarded by error estimates. The total length of undefined intervals amounts to 6.6% of the total outcrop length for the foot wall and to 8.4% for the hanging wall.

The *variogram* $\gamma_(\delta_j)$ at discrete scales $\delta_j \stackrel{\text{def}}{=} sj$ (s denotes the sampling interval)

$$\gamma_(\delta_j) \stackrel{\text{def}}{=} < [h_i - h_{i+j}]^2 > \tag{4.1}$$

is used to determine the fractal properties of roughness (Journel and Huijbregts 1978). In case of scaling invariance the variogram describes a power function

$$\gamma(\delta) \sim \delta^{\alpha} \tag{4.2}$$

which appears as a linear function

$$\log \gamma = \alpha \log \delta + \text{const.} \tag{4.3}$$

in a double logarithmic plot. The Hurst exponent H is directly related to the slope of this linear function by

$$\alpha = 2H \ . \tag{4.4}$$

Thus, the Hurst exponent is equal to half of the slope of the variogram in a double logarithmic plot. Interpretation might be biased towards scaling invariance if Hurst exponents are calculated over the entire scale interval. Natural fractures sometimes show different power law exponents at different scale ranges (Brown and Scholz 1985a). To study the constance of scaling, the considered scale range is divided into logarithmic scale bins with 2^n data points for which the Hurst exponents are calculated in advance. These Hurst exponents shall be called ”local” in to following since they only apply to restricted scale intervals rather than to the entire scale range.

Fault traces are divided into eight separate parts of equal length for which mean local Hurst exponents and standard deviations for the estimate of the mean value are calculated. The systematical error due to linear interpolation of undefined profile positions is regarded by the standard deviation, too. Linear trends are not removed from any of the eight sections to ensure that the mean Hurst exponents equal the Hurst exponents of the entire fault trace.

Local Hurst exponents of a fractal profile deviate from a constant value due to the artificial effect of limited sample size and detrending. To test whether local Hurst exponents of the fault sections are consistent with scale invariance, they will be compared to mean local Hurst exponents generated by fractional Brownian motion (fBm) on the basis of 1000 realizations. The Hurst exponents of the fBm-process are set to 0.8 and 0.9 to fit the measured values.

4.2.2 Results

The variograms of sections A, B, and C exhibit a general tendency towards a power law scaling of horizontal fault roughness (Figure 4.1). The drop off at large scales is attributed to the removal of the global linear trend.

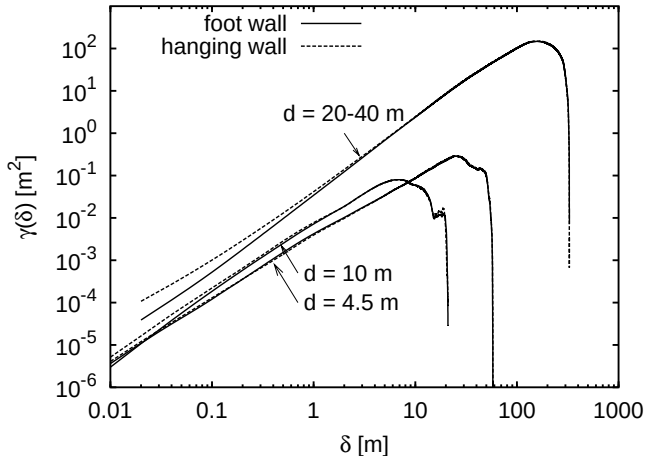

Fig. 4.1: Variograms for horizontal sections A, B, and C showing tendency to power law scaling.

Figures 4.2 and 4.3 show the mean values and standard deviations of the local Hurst exponents derived from the variograms of the splitted fault traces. Mean local Hurst exponents of fBm are displayed as lines.

Standard deviations increase with scale due to the decreasing number of height differences available for the calculation of variogram. The local Hurst exponents of the fault trace

measurements cover a broad scale range between 0.61 (rough) and 0.93 (smooth) which can partly be explained by the measuring method. At large scales, the Hurst exponents of both fault traces and fBm show a drop off which is related to the drop off of the variogram. Consequently, the increase of roughness with increasing scale, expressed by the decrease of H, is an artificial effect related to the fact that the whole profile has to be detrended in order to provide well defined measurement conditions.

The observed faults show significant deviations from fractal scaling (Figure 4.2 and 4.3) because the local Hurst exponents of fBm often do not lie within the standard deviation of the measured values. Especially the footwall of section A shows deviations that are in the order of several standard deviations.

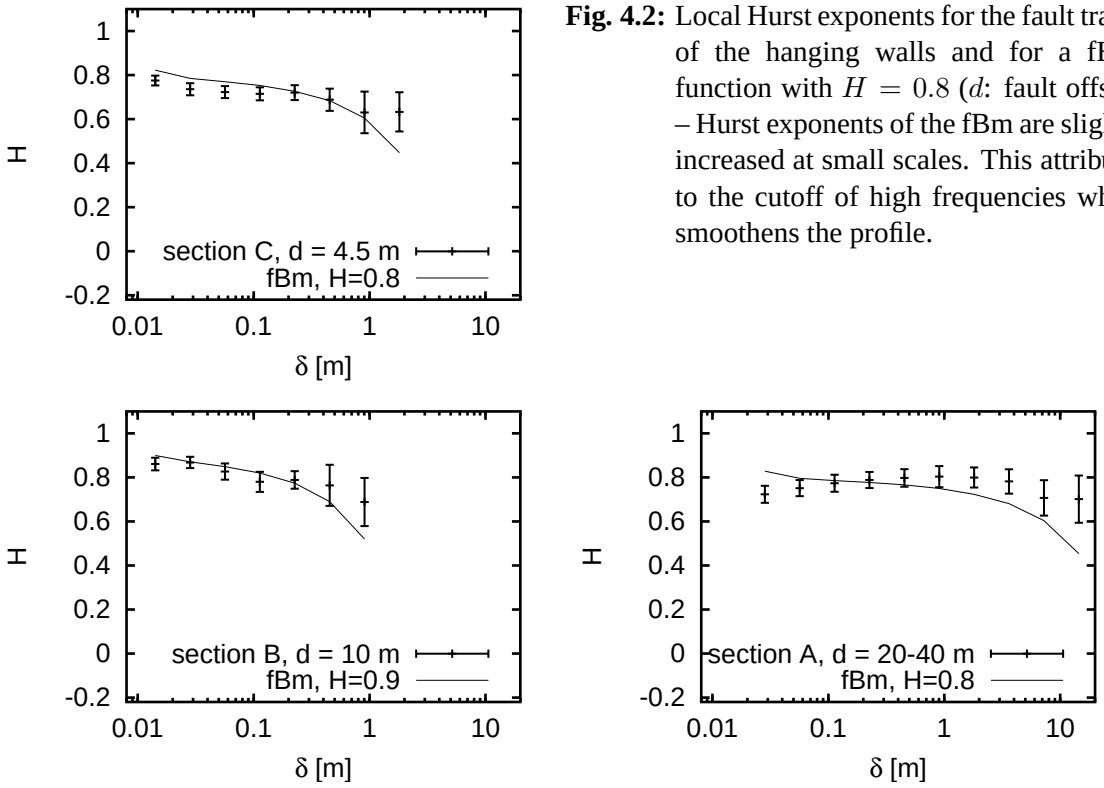

Fig. 4.2: Local Hurst exponents for the fault traces of the hanging walls and for a fBm-function with $H = 0.8$ (d: fault offset). – Hurst exponents of the fBm are slightly increased at small scales. This attributes to the cutoff of high frequencies which smoothens the profile.

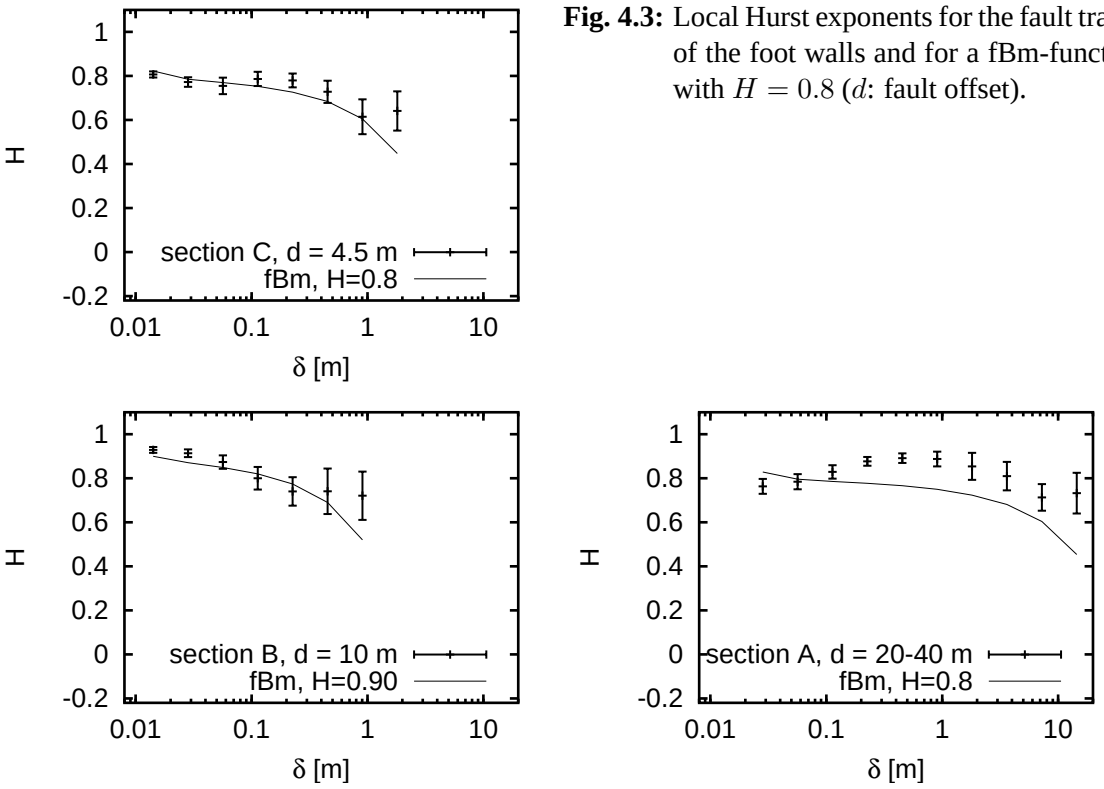

Fig. 4.3: Local Hurst exponents for the fault traces of the foot walls and for a fBm-function with $H = 0.8$ (d: fault offset).

4.2.3 Discussion

Despite the tendency towards a power-law scaling, the investigated fault sections do not show clean scale-invariance. Thus, they differ from experimental fractures, which have displayed self-affine, i.e. scale-invariant scaling in several studies. Many studies even state universal Hurst exponents in the sense that material and fracture mode has little influence on scaling behavior. Bouchaud (1997) points out in her review of fractal fracture analysis that Hurst exponents mainly depend on the speed of crack propagation: the studies of López and Schmittbuhl (1998), Schmittbuhl et al. (1995), Måløy et al. (1992), Bouchaud et al. (1990), Poon et al. (1992), McAnulty et al. (1992) concerning experimental fractures with fast crack propagation show Hurst exponents of approximately 0.8 whereas slow crack propagation results in rougher fractures with Hurst exponents around 0.6 (McAnulty et al. 1992). Obviously natural faults and fractures are more complicated and need not produce scale invariant fault topography.

The conclusion that natural fractures and faults need not be fractal is not new; there have been several observations of natural samples before, which have not shown any tendency towards universal scaling. Although the faults in sandstone and granite investigated by Power et al. (1987) and Schmittbuhl et al. (1993) have provided Hurst exponents of 0.75 and 0.84, respectively, the studies of Brown and Scholz (1985a) on natural joints in diabase and siltstone have yielded less univocal Hurst exponents ranging between 0.32 and 0.82. Most of these investigations have dealt with sample scales below 1 m because roughness data at field scale is difficult to obtain. The fractal analysis of this study shows that scaling invariance can also be questioned for natural faults at field scale.

Fractional Brownian motion (fBm) is an advanced approach to a description of natural faults and fractures since it accounts for the multi-scale aspect of roughness. Yet, the analysis has shown that faults are not exactly statistically similar to fBm. Differences between fBm and natural faults are obvious from a genetical point of view: fBm forms due to a stationary random process whereas natural fault topography is created by a multiplicity of different fracturing processes; this involves fracture coalescence and non-linear fracture propagation as was shown in the last chapter. This points out, that fBm is not the best solution for describing fault topography, and that natural faulting processes have to be taken into account again. With reference to fBm, faults are not fractal in general. Yet, fBm is only one example for fractal geometry, and possibly faults will provide some fractal characteristics if spatial distributions of certain segmentation types are considered.

4.3 Characteristic scales

4.3.1 Isotropic roughness measure

The length of a profile curve shall be used as an isotropic measure of fault roughness. Curve length is calculated by pacing off the fault trace with a ruler of length δ according to the classical method used to determine the fractal dimension of coast lines (Mandelbrot 1967). The curve length is equal to the number of required steps multiplied by the ruler length. If the size of the ruler δ is decreased the length of the curve $l(\delta)$ grows due to the influence of smaller corrugations. Thus, a scale dependent measure of roughness can be defined by

$$r(\delta) \stackrel{\text{def}}{=} -\frac{\mathrm{d}\log l}{\mathrm{d}\log \delta} \; . \tag{4.5}$$

This measure is chosen because

$$r = D - 1 \; . \tag{4.6}$$

for self-similar curves with fractal dimension D and $l \sim \delta^{1-D}$ (Feder 1988). Curve lengths are normalized by the distance between starting and ending points of a scan line. This provides a relative length $l'(\delta)$ which compensates variations of scan line length due to the fact that a measurement with a fixed ruler size usually does not span the entire curve. Ruler sizes are set to $s\,2^i$, where s denotes the sampling interval. For each scale the relative length is calculated by averaging over scan lines with varying starting points. The distance between adjacent starting points is in the range of the sampling interval. Positions between sample points are linearly interpolated.

To examine if the differences in the asymmetry of roughness between different exposures are statistically significant, the two longest fault sections A and C are divided in subsections of approx. 12 m length. Mean roughness values and standard deviations for the estimate of the mean values are calculated for all subsections of a fault (5 for section C and 25 for section A). The standard deviation account for roughness inhomogeneity as well as for systematical errors introduced by linearly interpolated subsections and measurement errors.

4.3.2 Results

Figure 4.4 shows the isotropic roughness r of sections A, B, and C. The ”local” fractal dimensions given by $D = r+1$ range between 1.0005 and 1.025 and are considerably smaller than those obtained by the Hurst exponents by $D = 2 - H$. This clearly demonstrates that scaling of fault roughness has a strong anisotropical component that cannot be detected by means of an isotropic measure.

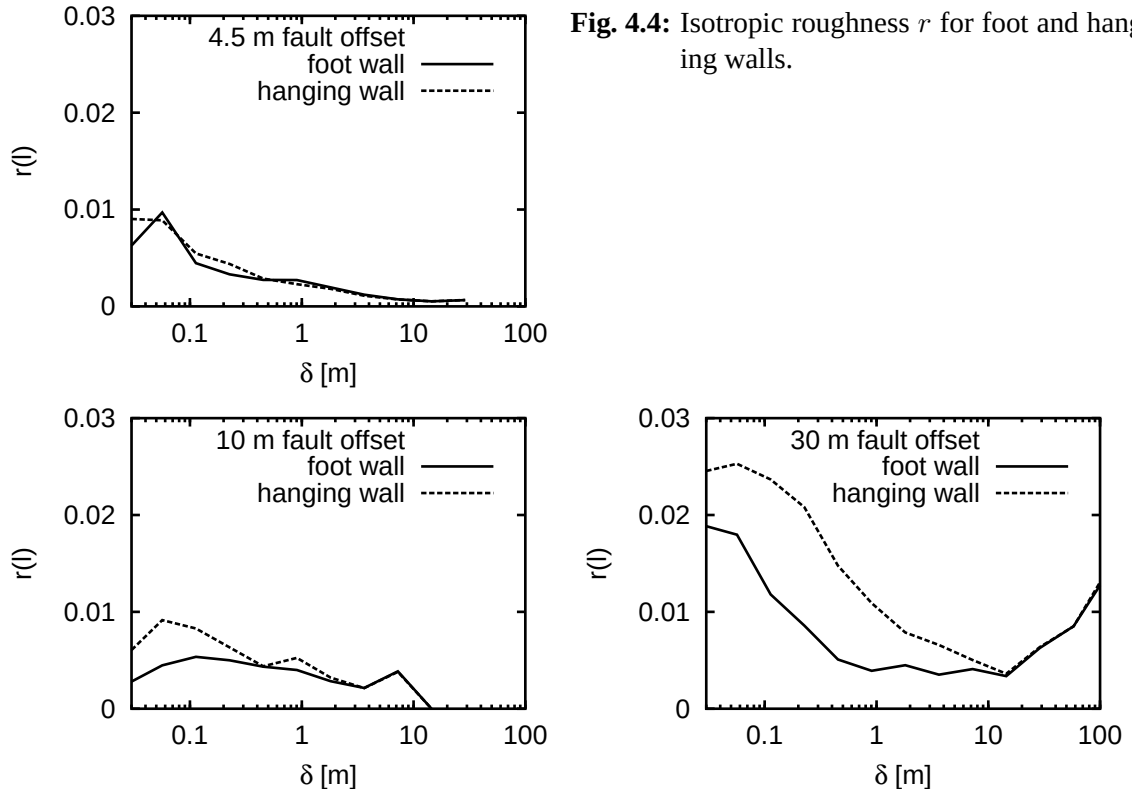

Fig. 4.4: Isotropic roughness r for foot and hanging walls.

The asymmetry of roughness that was noticed in Figure 4.4 shall be quantified by the relative roughness of the hanging wall, i.e. by the difference $\Delta r \stackrel{\text{def}}{=} r_{\text{h}} - r_{\text{f}}$, where r_{h} and r_{f} denote the isotropic roughness of the hanging wall and foot wall, respectively. According to Figure 4.5, the intensity and maximum scale of asymmetry increase with fault offset. Figure 4.6 shows the error estimates of roughness asymmetry for sections A and C. Obviously, the difference in roughness asymmetry is significant, at least for these two sections.

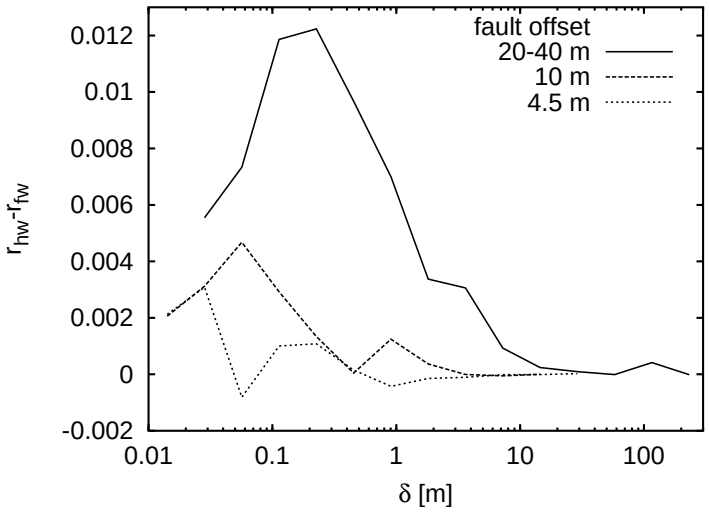

Fig. 4.5: Asymmetry of isotropic roughness Δr.

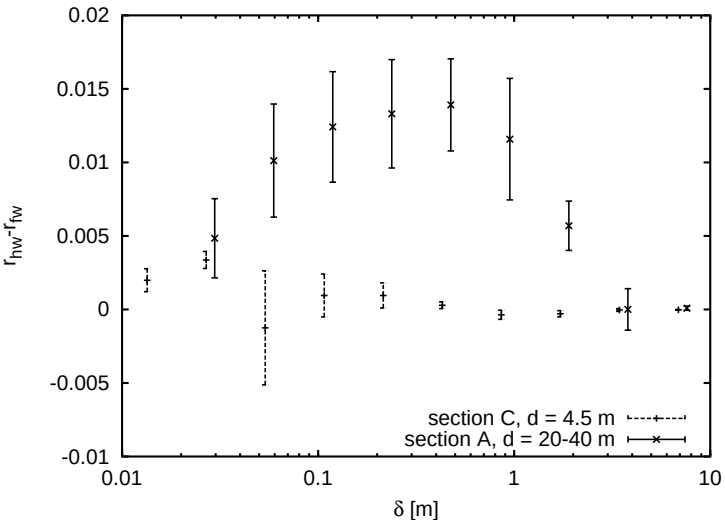

Fig. 4.6: Mean asymmetry of isotropic roughness Δr of section A and C for 12 m long subsections 12 m.

4.3.3 Discussion

On the basis of the field observations, the asymmetry of isotropic roughness is best explained by the asymmetrical occurrence of secondary damage structures. It was shown that detachment of lignite fragments from the fault wall leads to a considerable increase of fault thickness. Consequently, this mechanism is able to produce high roughness amplitudes at small scales which can be detected by a measurement of roughness. The proposed correlation between lignite detachment and characteristic scale of roughness asymmetry agrees with the findings of Lee and Bruhn (1996) who studied scaling properties of normal faults in limestone and quartzite. The authors report several characteristic scales of roughness, especially when measured perpendicular to the slip direction. They assume that scaling properties at scales around 1 m reflect a combination of frictional ploughing (by asperities) and secondary fracturing. Secondary faults in limestone, possibly corresponding to the splay faults of this study, were suggested to sign responsible for the strong corrugations of the fault surface.

However, the reliability of the correlation between characteristic scale of roughness and damage process is not fully contenting. A more compellent correlation would require a spatial resolution of roughness asymmetry, for instance by wavelet or windowed Fourier analysis, and a study of the structural phenomena at locations with asymmetrical roughness. This proceeding was not possible in this study because mining activity allowed only short access to the fault exposures. Additionally, the fault exposures were too narrow for quantitative investigation of fault wall damage.

Provided that damage signs responsible for the asymmetry of roughness, the scale of asymmetry should reflect the size of detachment zones. Indentations in the fault wall produced by lignite detachment will provide the highest roughness if the ruler size is about half the size of the indentation. Thus, the size of the detachment zones measured parallel to the fault strike is about twice the size of the characteristic scale of asymmetry. The increasing scale of asymmetry indicates an increasing size of detachment zones. This need not imply that large damage zones are formed at large offsets. A scale increase can also be achieved by simply extending existing damage zones. In every case, the size of detachment zones and the mean width of the main shear zone increase with fault offset. This suggests that characteristic scales of roughness are introduced by fault offset even if all processes of fault nucleation should produce fractal fault surfaces. Since fault offset is alway small compared to the fault size, fault should always show scale domains with different scaling of roughness.

Chapter 5

Numerical fault model

5.1 Purpose

Several indications for the existence of vertical fault roughness have been presented in the previous chapters, encompassing the variability of horizontal roughness or the occurrence of secondary structures related to spatially inhomogeneous friction, like splay faults or fragmentation zones. Vertical roughness probably signs responsible for the increasing size of detachment zones with increasing fault offset that was found by the fault trace analysis. Still, we do not know how vertical roughness controls the formation of damage structures because quantitative data of vertical roughness is not available.

A numerical fault model is introduced to study how scale and intensity of damage is controlled by multi-scale roughness and mechanical rock parameters. Rough fault surfaces are generated by the stochastical process of fractional Brownian motion (Figure 5.1). A shear experiment is repeated several times using different realizations of fault surfaces (Figure 5.2). This affords a strong simplification of mechanical processes. Thus, the damage process chosen for the model is that of minimal damage necessary to maintain slip.

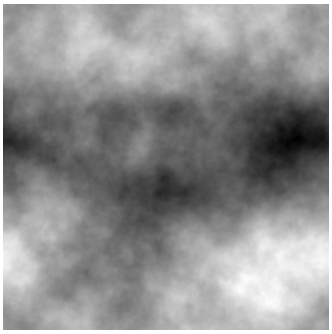

Fig. 5.1: Fault surfaces are represented as fractal surfaces in the numerical fault model (elevated regions are shaded dark).

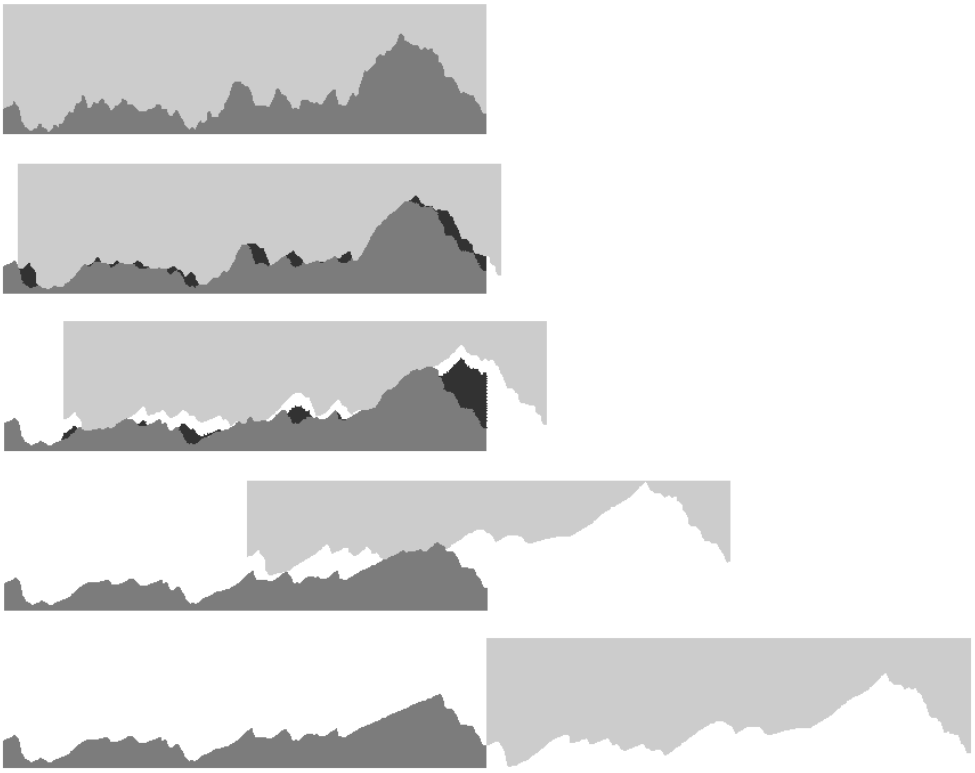

Fig. 5.2: Illustration of the model configuration (section in slip direction). The upper surface is shifted to the right during the shear experiment. Asperity summits are eroded and the detached material (dark grey) is trapped between the fault surfaces. Decreasing area of surface opposition leads to a loss of fault gouge material (part of gouge material is hidden in other sections).

5.2 Physical description

Fault surfaces. Two rough surfaces of finite length L shall simulate a fault zone within a brittle layer which is embedded in soft rock. The initial roughness shall follow a fractional Brownian motion process (fBm) which is fully determined by its power spectral density

$$P(f) \stackrel{\text{def}}{=} P_{\frac{1}{L}} \cdot (Lf)^{-\beta}$$

where $P_{\frac{1}{L}}$ is the power spectral density at frequency $\frac{1}{L}$. The power-law exponent β is determined by the Hurst exponent H due to the relation $\beta = 2H + 1$ for $0 < H < 1$. The power spectral density $P_{\frac{1}{L}}$ at frequency $\frac{1}{L}$ shall be determined by the roughness amplitude

$$A_{\frac{1}{L}} \stackrel{\text{def}}{=} \sqrt{\int_{\frac{1}{L}}^{\infty} P(f)df} = \sqrt{\frac{P_{\frac{1}{L}}}{L(\beta-1)}} = \sqrt{\frac{P_{\frac{1}{L}}}{2HL}} \, .$$

For further considerations, roughness amplitudes shall be small relative to the profile length according to the field observation that vertical roughness has low amplitudes.

Stress boundary condition. In every tectonic regime, the principle stress axes of the global stress field near the earth surface are aligned horizontally and vertically. The vertical principle stress remains constant if no significant sedimentation or erosion takes place. Tectonic extension decreases the horizontal principal stress until fracturing takes place and extension can be compensated by normal faulting. The global stress field changes on a large time scale whereas slip events happen at small time scales. This allows a separation of time scales leading to a constant approximation of the global stress field. We therefore assume a constant mean normal stress $\bar{\sigma}^{\perp}$ on the fault surface.

Slip. Fault slip shall be regarded as a creeping movement without significant participation of kinetic energy. This is a major simplification since stick slip is a common phenomenon of natural fault activity and even present in granular material (Nasuno et al. 1998, Chain et al. 2001) where strain rate dependent fault zone dilatancy counteracts velocity weakening effects necessary for stick slip (Rice 1983, Rudnicki 1988). However, the study focuses on the geometrical effect of fault roughness on damage. A strong simplification of the mechanical processes is necessary to perform a large number of shear experiments with different realizations of fault surfaces with multi-scale roughness.

Assuming that only few fault locations are interlocked at a time, fault offset shall be described by a kinematic boundary condition. If there is a large area with relatively low

frictional resistance, it will control the subsidence of the hanging wall, thereby imposing a kinematic boundary condition on the interlocked parts of the fault. The assumption of a large area of low friction is reasonable for the investigated faults which mainly cut through sand layers where fault roughness and thus the probability of interlocking asperities is lower than in lignite.

Material phases. The rock shall be described by a 2-phase system. The first phase is the intact rock, the second the grinded material that is detached from the fault walls and trapped inside the fault gouge (which here refers to the space between the fault surfaces). The rock itself will not be modeled. Instead, mechanical properties of the rock will be simulated by properties of the fault surfaces.

Mechanical properties of the intact material. These are the mechanical properties of the intact rock and the corresponding representation by surface properties:

- The rock shall behave like an ideal elastic medium. Elasticity is described by a linear relationship between stress and surface displacement $\Delta h \sim \sigma$. From this we define a compression modulus D for which the height change is

  $$\Delta h = D\,\sigma \ .$$

  Since roughness amplitudes are assumed to be small and slip parallel movement is controlled by a kinematical boundary condition, strain parallel to the fault plane can be neglected. The compression modulus for normal stress parallel to the fault plane is therefore set to zero. This allows the use of an equidistant grid for the numerical model which drastically reduces the numerical effort.

- The rock shall break according to the Mohr-Coulomb criterion for shear failure. The failure criterion is controlled by the cohesion c and internal friction angle ϕ of the rock. Fracturing takes place, if there is a hypothetical fracture plane for which shear stress τ and normal stress σ satisfy

  $$\tau \geq c + \sigma \tan\phi \ . \tag{5.1}$$

- Contacting parts of the fault walls shall exhibit stiction. To initiate slip at such an "interlocked" location, shear stress τ^{cs} and normal stress σ^{cs} on the contact surface must satisfy

  $$\tau^{\mathrm{cs}} \geq \mu\sigma^{\mathrm{cs}} \ , \tag{5.2}$$

  where μ denotes the friction coefficient.

Mechanical properties of the grinded material. The grinded material is modeled as a friction-less fluid to avoid modeling shear stresses within the fault gouge material. The grinded material will flow freely within the fault gouge towards places with minimal pressure. Since straining of grinded material will not produce any shear stress, no shear failure will occur where grinded material is present. For this reason this phase will be called "lubricant" in the following.

Damage and wear. The process of abrasive wear describes the transition between the two material phases, intact rock and lubricant. Wear is initiated if local stresses satisfy the shear failure criterion. The model simulates *minimal damage* necessary for a slip of the entire fault block. If the inclination of a local contact surface relative to the global slip direction is too high to enable slip before the rock begins to fail, only that amount of rock will be fragmented and detached from the fault walls that decreases the surface inclination to the maximal value necessary for fault slip. The concept of minimal damage in a 2-phase system implies that the phase boundary between intact rock and lubricant is sharp and propagates slowly through the rock. What speaks in favor of the concept of minimal damage is the fact that the extent of damaged rock can be determined within the physical model, which does not resolve shear stresses. Strictly speaking, minimal damage only alters the fault walls but does not produce any damage zones because the fragmented material is immediately transferred to the fault gouge.

Friction in natural rock is controlled by several types of asperity interactions. Scholz (1990) distinguishes ploughing of asperities, sliding up of asperities causing fracture dilatancy, and interlocking with shearing through asperities. All these processes raise friction coefficients above the value of $\mu = \frac{1}{6} \approx 0.15$ predicted by the adhesion theory of friction for ideally plastic material (Bowden and Tabor 1950, 1964). The sliding-up mechanism, which is described by the assumption of minimal wear, is suppressed at high normal stresses because the asperities cannot withstand the stress concentration caused by the reduction of contact area. Asperities fail brittle or plastically and shearing through asperities becomes the dominant process of abrasive wear. Thus, the model describes the wear processes only for low normal stresses at which sliding up of asperities is still possible.

5.3 Model simplification

The physical model described above depends on seven parameters: the global normal stress $\bar{\sigma}^{\perp}$, the material parameters c, ϕ, μ, D, and the surface parameters H and $A_{\frac{1}{L}}$. A rescaling of parameters and a simplification of the wear process will allow to reduce the number of model parameters to three.

Wear. In the following, we will consider the inclination of contact surfaces resulting from shear failure. If shear failure takes place, shear stress τ^{y} and normal stress σ^{y} on the failure surface follow

$$\tau^{\mathrm{y}} = c + \sigma^{\mathrm{y}} \tan\phi \tag{5.3}$$

according to the Mohr-Coulomb criterion. σ^{y} and τ^{y} can be written in terms of the minium and maximum principle stresses $\sigma^{\min}$ and $\sigma^{\max}$ as

$$\sigma^{\mathrm{y}} = \frac{\sigma^{\max} + \sigma^{\min} + (\sigma^{\min} - \sigma^{\max})\sin\phi}{2} \quad \text{and} \quad \tau^{\mathrm{y}} = \frac{\sigma^{\max} - \sigma^{\min}}{2}\cos\phi\,. \tag{5.4}$$

At sticked contact zones, the orientation of the maximum principle stress axis probably ranges between that of the global stress field and an inclination of 45° to the fault plane if the subsidence of the hanging wall induces fault parallel shear strain. To simplify the model, we assume that the local minimum and maximum principle stress axes are always parallel to those of the global stress field. This says that failure surfaces are aligned parallel to the global orientation of the main fault. According to this assumption, shear stress and normal stress on the contact surface are given by the equations

$$\tau^{\mathrm{cs}} = \frac{\sigma^{\max} - \sigma^{\min}}{2}\cos(\phi - 2\beta) \tag{5.5}$$

$$\text{and} \quad \sigma^{\mathrm{cs}} = \frac{\sigma^{\max} + \sigma^{\min} + (\sigma^{\min} - \sigma^{\max})\sin(\phi - 2\beta)}{2}\,, \tag{5.6}$$

where the angle β denotes the inclination of a local contact surface to the slip direction (Figure 5.3). Together with 5.3 and 5.4, and using the relation $\frac{\sigma^{\max}+\sigma^{\min}}{2} = c\tan\phi + \sigma^{\mathrm{y}}(1 + \tan^2\phi)$ they turn into

$$\tau^{\mathrm{cs}} = (c + \sigma^{\mathrm{y}}\tan\phi)\frac{\cos(\phi - 2\beta)}{\cos\phi} \tag{5.7}$$

$$\text{and} \quad \sigma^{\mathrm{cs}} = c\tan\phi + \sigma^{\mathrm{y}}(1 + \tan^2\phi) - (c + \sigma^{\mathrm{y}}\tan\phi)\frac{\sin(\phi - 2\beta)}{\sin\phi} \tag{5.8}$$

According to the concept of minimal damage, β is given by the surface angle for which slip coincides with the onset of shear failure. If this is the case, shear and normal stress on the contact surface are related by

$$\tau^{\mathrm{cs}} = \mu\sigma^{\mathrm{cs}}\,.$$

Together with 5.7 and 5.8 and using trigonometrical addition theorems we obtain the maximal yield slope as

$$\tan\beta = \frac{1}{\cos\phi + \mu\sin\phi + b}(\sin\phi - \mu\cos\phi + \sqrt{1 + \mu^2 - b^2}) \tag{5.9}$$

$$\text{where} \quad b \stackrel{\text{def}}{=} \mu \frac{c \sin\phi \cos\phi + \sigma^{\text{y}}}{c \cos\phi + \sigma^{\text{y}} \sin\phi} \; .$$

For stresses very much higher than the cohesion, i.e. for $\sigma^{\text{y}} \tan\phi >> c$, the maximal slope is nearly independent from stress since $b \approx \frac{\mu}{\sin\phi}$ (it shall be noted here, that the friction coefficient of the entire fault is still dependent on normal stress). For the investigated faults, the mean stress of about 6 MPa at 200 m depth at time of faulting approximately satisfied this condition for a cohesion and internal friction angle of $c = 0.2$ MPa and $\phi = 30°$ (personal communication with *Rheinbraun*). However, high normal stresses cannot be guaranteed for all surface contacts if the surfaces are rough even if the mean normal stress is high. Yet, a consideration of how β changes with stress shows that the approximation of a constant slope is reasonable. Figure 5.4 displays the difference of yield angle and limit yield angle $\beta - \lim_{\sigma^{\text{y}} \to \infty}(\beta)$ as a function of σ^{y} for different values of μ. Yield angles remain quite constant especially if the friction coefficient μ is smaller than the slope of the internal friction angle $\tan\phi$. For $\mu \leq 0.75 \tan\phi$, significant deviations of the yield angle from a constant value only occur within a narrow stress interval.

How large is the friction coefficient at an asperity contact after damage has taken place? According to Byerlee (1978) friction coefficients are about 0.85 for normal stresses below 200 MPa and 0.6 for normal stresses above 200 Pa independent of rock type (*Byerlees's law*). At the first sight, this seems to contradict the assumption of $\mu \leq \tan\phi \approx 0.58$ for $\phi = 30°$. Yet, Byerlee (1978) determined the friction coefficients primarily for rough mated fractures. As was mentioned before, asperity interactions increase the macroscopic friction coefficient above the value of $\frac{1}{6}$ predicted by the adhesion theory for ideally plastic material. The great influence of roughness on friction coefficients is underlined by the experiments of Byerlee (1967) with smooth unmated surfaces which yielded values between 0.2 and 0.6. We have to note that the friction coefficient μ used in the model does not refer to the macroscopic friction coefficient of the entire fault which is high due to fault roughness. Instead, μ describes the microscopic behavior at the asperity contact where damage takes place until shear strain

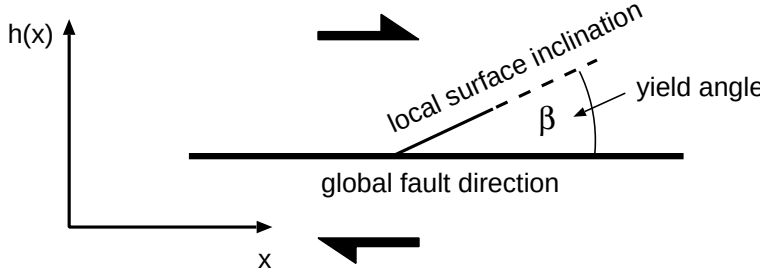

Fig. 5.3: Definition of the yield angle β.

or slip sets on to overcome the obstacle. Consequently, the evolving microscopic shear zone is a broad zone of fragmentation which should approximately behave like a plastic granular material. Thus, it can be expected that μ is near the value of $\frac{1}{6}$ for plastic material. The approximation of constant yield angles should therefore be adequate for most surface contacts. The parameters c, ϕ, and μ will therefore be substituted by the yield slope $\tan\beta$.

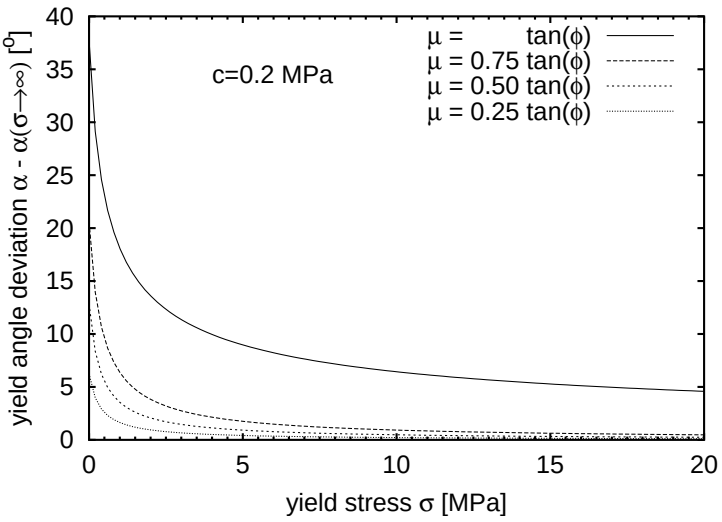

Fig. 5.4: Difference of yield angle and limit yield angle as a function of yield stress σ^{y}.

Rescaling. Rescaling of parameters provides a set of three independent model parameters. First, the yield slope $\tan\beta$ will be substituted by a relative yield slope α

$$\tan\beta \quad \longmapsto \quad \alpha \stackrel{\text{def}}{=} \frac{\tan\beta}{\frac{A_{\frac{1}{L}}}{L}}$$

which is now coupled to the roughness amplitude. The normation by $A_{\frac{1}{L}}/L$ is chosen because increasing the relative roughness amplitude $A_{\frac{1}{L}}/L$ is equivalent to reducing the slope α by the same factor. Consequently, materials with low β have a low yield strength, a high friction coefficient or high roughness amplitudes.

Compression modulus, mean normal stress and roughness amplitude control the closure of the fault surface by linear elastical strain. They can be substituted by a mean relative strain δ by

$$D\bar{\sigma}^{\perp} \quad \longmapsto \quad \delta \stackrel{\text{def}}{=} \frac{D\bar{\sigma}^{\perp}}{A_{\frac{1}{L}}} \ .$$

Final parameter set. Due to rescaling and a simplification of the wear process, the system is now controlled by the three dimensionless parameters

α	relative yield slope
H	Hurst exponent
δ	mean relative strain

5.4 Numerical model

Fault surfaces. The fault is represented by two horizontal fault surfaces. During fault displacement, the upper surface is shifted to the right. Fault surfaces are described by two-dimensional discrete functions of relative height $h^{\mathrm{u}}_{i,j}$ and $h^{\mathrm{l}}_{i,j}$ for the upper and lower surface, respectively. Relative heights shall be defined as surface heights divided by the roughness amplitude $A_{\frac{1}{L}}$. The height functions $h^{\mathrm{u}}_{i,j}$ and $h^{\mathrm{l}}_{i,j}$ are defined on an equidistant grid with $0 \leq i \leq n-1$ and $0 \leq i \leq n-1$ with a side length $L = 1$.

Every shear experiment starts with equal height functions $h^{\mathrm{u}} = h^{\mathrm{l}}$. The initial roughness is generated by the process of fractional Brownian motion with a Hurst exponent $H \in]0;1[$ and a roughness amplitude $A_{\frac{1}{L}} = 1$.

During fault offset the upper surface is raised relatively to the original position as a consequence of surface roughness. For a relative lift l, the actual heights of the raised upper surface are given by $h^{\mathrm{u}}_{i,j} + l$.

Fault displacement. Fault offset is controlled kinematically by a right shift of the upper surface by one grid point (in direction of the index j). For a fault offset o, which shall be defined as an index offset with $0 \leq o \leq n-1$, the opposing parts of both surfaces are given by the index spaces

$$I^{\mathrm{l}} \stackrel{\mathrm{def}}{=} \{i,j \quad | \quad 0 \leq i \leq n-1 \quad \wedge \quad o \leq j \leq n-1\}$$

for the lower surface and by

$$I^{\mathrm{u}} \stackrel{\mathrm{def}}{=} \{i,j \quad | \quad 0 \leq i \leq n-1 \quad \wedge \quad 0 \leq j \leq n-1-o\}$$

for the upper surface.

Fault gouge material. The relative thickness of the lubricant above a location (i,j) of the lower surface is denoted by $u^{\mathrm{l}}_{i,j}$ (the literal u^{l} shall refer to a thickness in the following). The total amount of lubricant present in the fault gouge is given by

$$U^{\mathrm{l}} \stackrel{\mathrm{def}}{=} \sum_{(i,j) \in I^{\mathrm{l}}} u^{\mathrm{l}}_{i,j} \ .$$

U^{l} will be called the cumulative relative thickness of the lubricant in the following. With every height change of a fault surface location due to wear it grows by the same amount.

During fault displacement the area of surface opposition decreases to zero. With every displacement step the cumulative relative thickness of the lubricant U^{l} is reduced by half of the lubricant volume stored at the uttermost locations of the fault gouge:

$$U^{\mathrm{l}} \quad \longmapsto \quad U^{\mathrm{l}} - \frac{u^{\mathrm{l}}_{i,o} - u^{\mathrm{l}}_{i,n-1}}{2} \; .$$

To study the influence of the lubricant on damage, the lubricant can be removed from the fault gouge by setting $U^{\mathrm{l}} = 0$.

Lubricant distribution. To determine the relative lift l of the upper surface for a given fault offset the distribution of the lubricant $u^{\mathrm{l}}_{i,j}$ must be known. The distribution is controlled by the ability of the lubricant to flow to places of lowest normal stress.

The distribution of the lubricant depends on the relative lift of the upper plate l and the relative lift l_0 for which the volume in between the fault surfaces equals the lubricant volume. Three cases have to be distinguished. If $l > l_0$, the fault gouge volume (i.e. the volume in the area of surface opposition) is larger than the lubricant volume. Due to the high mobility, the lubricant will escape from all locations of surface contact. The distribution of lubricant will not be relevant in this case because it neither influences the local normal stresses nor the decision for asperity failure. If $l = l_0$, the lubricant occupies the entire space between the fault surfaces but the normal stress on the lubricant is still zero at all locations and nothing will happen here, too. In case of $l < l_0$, the distribution of lubricant shall be set equal to the state at $l = l_0$. This resembles the fact that all the lubricant has flown to the place of lowest normal stress.

Lift of the upper surface and surface deformation. The relative lift l of the upper plate is searched iteratively until the boundary condition given indirectly by δ is met. To find l, the critical lift l_0 for which the lubricant volume equals the fault gouge volume has to be calculated. In this case

$$U^{\mathrm{l}} = \sum_{(i,j)\in I^{\mathrm{l}}} u^{\mathrm{ap}}_{i,j} \; ,$$

where

$$u^{\mathrm{ap}}_{i,j}(l) \stackrel{\mathrm{def}}{=} \rho(h^{\mathrm{u}}_{i,j-o} + l - h^{\mathrm{l}}_{i,j}) \quad \text{with} \quad \rho(x) = \begin{cases} x & x > 0 \\ 0 & x \leq 0 \end{cases}$$

is the local relative aperture between the lower surface and the lifted upper surface. Calculation of l_0 is done iteratively. If l_0 is finally found, the local relative lubricant thickness is set to

$$u^{\mathrm{l}}_{i,j} = u^{\mathrm{ap}}_{i,j}(l_0) \; .$$

In advance, the relative lift l is searched iteratively. For a given relative lift, the change of relative surface height due to compression $u^{\mathrm{c}}_{i,j}$ is given by

$$u^{\mathrm{c}}_{i,j}(l) \stackrel{\mathrm{def}}{=} \frac{1}{2}\rho(h^{\mathrm{l}}_{i,j} - h^{\mathrm{u}}_{i,j-o} - l + u^{\mathrm{l}}_{i,j}) \; . \tag{5.10}$$

The actual lift is found if

$$\frac{1}{m(n-o)} \sum_{(i,j)\in I^{\mathrm{l}}} u^{\mathrm{c}}_{i,j}(l) A_{\frac{1}{L}} = D\bar{\sigma}^{\perp}$$

which is equivalent to

$$\frac{1}{m(n-o)} \sum_{(i,j)\in I^{\mathrm{l}}} u^{\mathrm{c}}_{i,j}(l) = \delta \; .$$

With l, the deformed fault surfaces $\hat{h}^{\mathrm{u}}$ and $\hat{h}^{\mathrm{l}}$ are calculated by

$$\hat{h}^{\mathrm{l}}_{i,j} = h^{\mathrm{l}}_{i,j} - u^{\mathrm{c}}_{i,j}(l) \quad \text{and} \quad \hat{h}^{\mathrm{u}}_{i,j} = h^{\mathrm{u}}_{i,j} + u^{\mathrm{c}}_{i,j}(l) \; .$$

Asperity failure. Before the upper plate is shifted by one grid point, each surface location having contact to the opposing surface is checked, whether it will slip or break. This is done by comparing the local relative slope $\frac{h^{\mathrm{l}}_{i,j+1} - h^{\mathrm{l}}_{i,j}}{1/n}$ with the relative yield slope α. If the local relative slope exceeds the relative yield slope, the fault is unable to slip at this location and $h^{\mathrm{l}}_{i,j+1}$ and $h^{\mathrm{u}}_{i,j}$ are altered until the local slope equals the yield slope (Figure 5.5). Wear is calculated for all locations on the basis of the unaltered surfaces to make the process independent from the order of indices at which wear takes place. The change of relative heights caused by wear is added to the cumulative relative thickness of the lubricant U^{l}.

5.5 Parameter space

To study the influence of model parameters, a central parameter set is defined according to Table 5.1, and single parameters are varied while all others are kept constant.

For the central data set, a Hurst exponent of $H = 0.8$ is chosen, which is a commonly measured value for experimental fractures. H will be varied between 0.3 and 0.9. The central value for the relative yield slope is set to $\alpha = 0$, which is the only value that allows wear at all scales independent of the fractal characteristic (for $\alpha > 0$ there is always a scale above which slopes are so small that no damage will take place). α will be successively increased to 80, a value for which almost all wear activity ceases for $H = 0.8$.

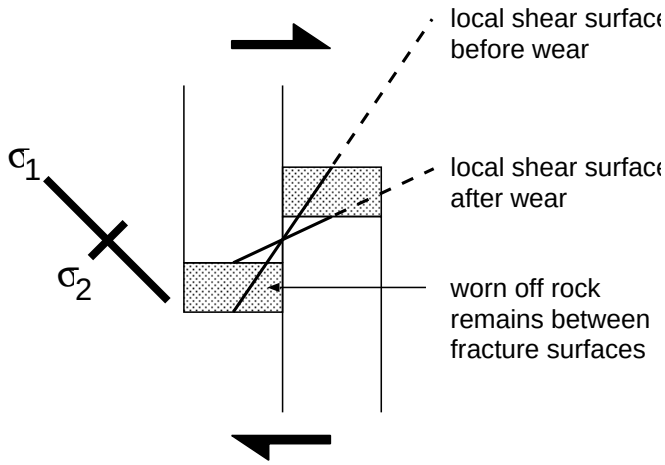

Fig. 5.5: Wear at interlocked asperities. – Wear takes place if the fracture criterion is reached due to a stress increase before slip happens. The new slip surface is determined by the maximum angle that allows slip at fracture stress.

For $A_{\frac{1}{L}} = 1$ the mean difference between maximal and minimal surface height ranges between 11.26 and 11.69 for Hurst exponents of 0.9 and 0.3, respectively. So, a mean relative strain δ of 100 will be sufficient to avoid empty space within the fault gouge. In this case the topography of the compressed surfaces is independent from the mean relative strain. To study the influence of low compression, the mean relative strain will also be considered at $\delta = 0.1$.

Tab. 5.1: Central parameter set

Parameter		central value	range
Number of grid points	n	256	128 to 1024
No. surfaces per test		1000	
Hurst exponent	H	0.80	0.30 to 0.90
Relative yield slope	α	0	0 to 80
Mean relative strain	δ	100	0.1 and 100
Lubrication		on	on and off

5.6 Results

5.6.1 Central parameter set

Figure 5.6 shows how fault topography and damage field (i.e. the height change relative to initial topography) evolves during fault offset. The fault surface becomes anisotropic and shows lineation typical for natural slip surfaces. The damage field seems to be isotropic at the first sight. Both, the scale of lineation and the scale of damage increase with offset. There is an apparent correlation between the fractal properties of the initial heights and the evolving damage field.

Fractal properties are characterized by means of variograms of the height and damage fields in direction parallel and perpendicular to slip. Figure 5.7 (top) displays variograms of the damage field at logarithmic steps of fault offset together with the variogram of the initial height field. During offset the variogram of the damage field gradually approximates the variogram of the height field. Equality would be reached if the wear process would produce plane fault surfaces. Approximation to this state begins with small damage scales and affects ever larger scales with increasing fault offset. Damage activity ceases if either the maximal offset is reached or if lubrication prevents further damage. Variograms (Figure 5.7 top) and variogram slopes (Figure 5.7 bottom) indicate that this happens before the damage field has reached the fractal scaling of the initial fault surface. The resulting damage field is therefore rougher than the initial fault surface in terms of scaling. Roughness evolves more slowly perpendicular to slip direction, which produces a slight anisotropy of the damage field that is not apparent from the images of Figure 5.6. An upper limit to the scale of damage is given by the size of the fault because it determines the available frequency spectrum of roughness and the maximal offset.

As Figure 5.7(top) shows, the increase of roughness is strongest at small fault offsets. This shall be measured by the *wear activity*

$$w(o) \stackrel{\text{def}}{=} \frac{U^1(o)}{\frac{m(n-o)}{mn}\frac{1}{n}} - \frac{U^1(o-1)}{\frac{m(n-o-1)}{mn}\frac{1}{n}} ,$$

which is the mean relative wear height per area of surface opposition and relative displacement step. Figure 5.8 points out that most of the wear takes place at small offsets. The drop off of wear activity can either be caused by decreasing roughness amplitudes or by an increasing mismatch of the opposing fault surfaces that reduces the total contact area.

In the following sections, model parameters will be varied from the central dataset. The scaling of roughness will be studied by means of variograms of initial fault topography and final damage field. To compare the duration of wear for different parameter sets, a *normal*

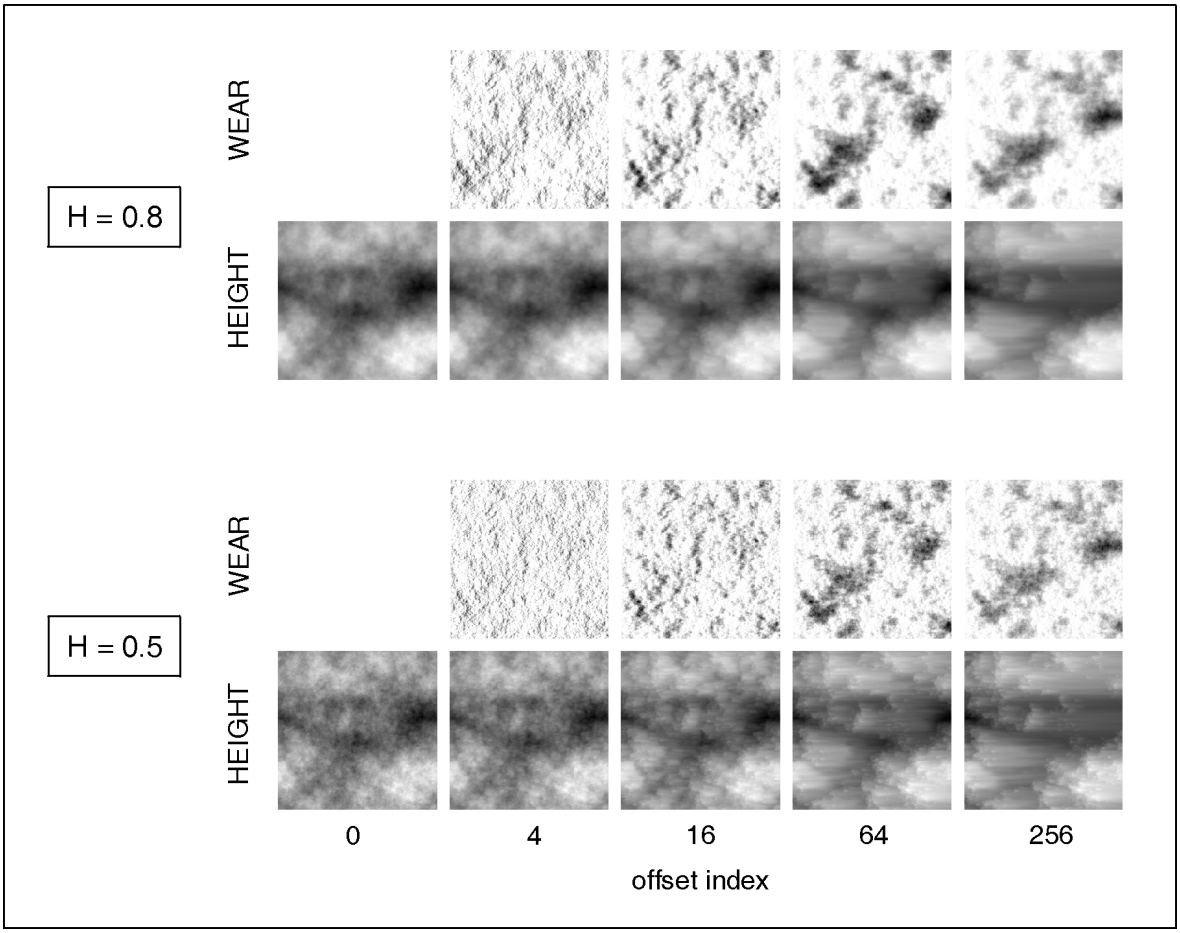

Fig. 5.6: Evolution of surface height and height change due to damage (view on lower surface from above; raised positions are colored black). The upper surface was shifted to the right.

wear activity $\hat{w}$ is defined by rescaling the wear activity in the way that the area beneath the function equals 1:

$$\hat{w}(o) \stackrel{\text{def}}{=} (n-1)w(o)\left(\sum_{1\le i\le n-1} w(i)\right)^{-1}$$

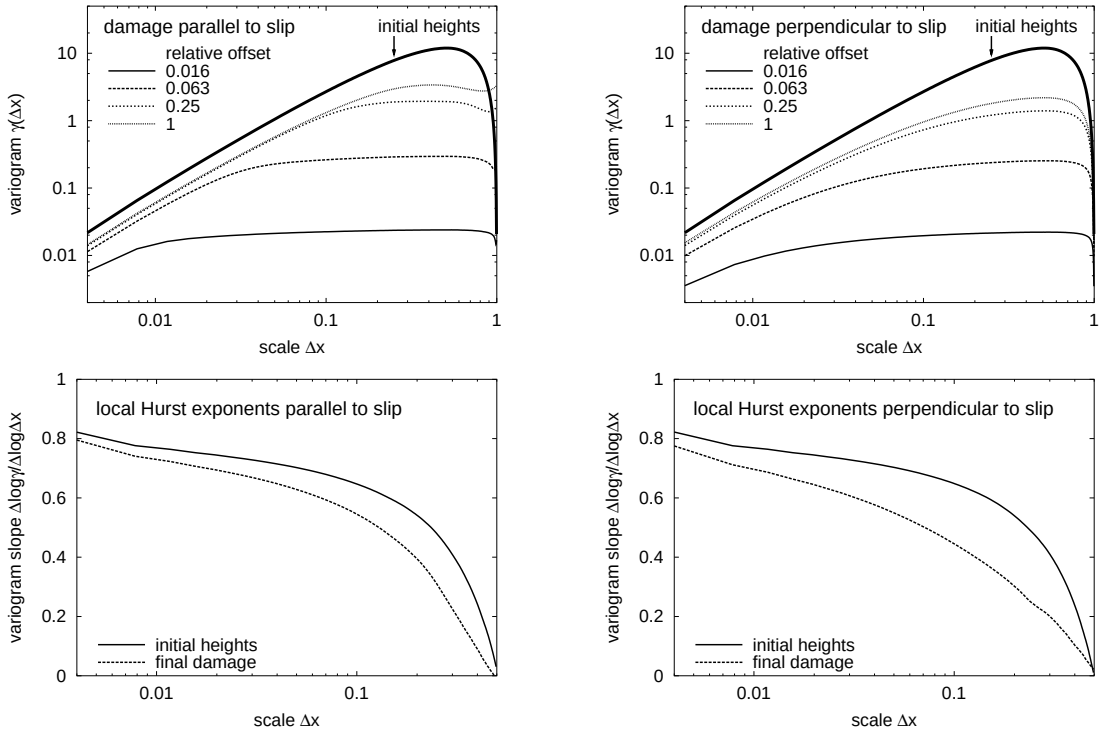

Fig. 5.7: *Top:* Variograms for different fault offsets. Variograms were measured over the entire fault surface including parts without surface opposition (Variograms of the damage field need not drop off at large scales because profiles are not detrended). *Bottom:* Half variogram slopes of initial heights and final wear fields, reflecting "local" Hurst exponents.

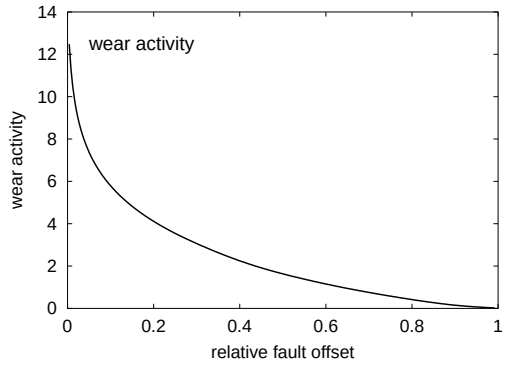

Fig. 5.8: Wear activity (change of relative height per area of surface opposition) for the central parameter set.

5.6.2 Variation of grid size

The influence of grid size is assessed by model runs with $n = 128$, $n = 256$, $n = 512$, and $n = 1024$. As Figure 5.9 shows, the grid size has little influence on the model behavior, neither on wear activity, nor on the scaling of roughness. Thus, a finer discretization than $n = 256$ is not necessary.

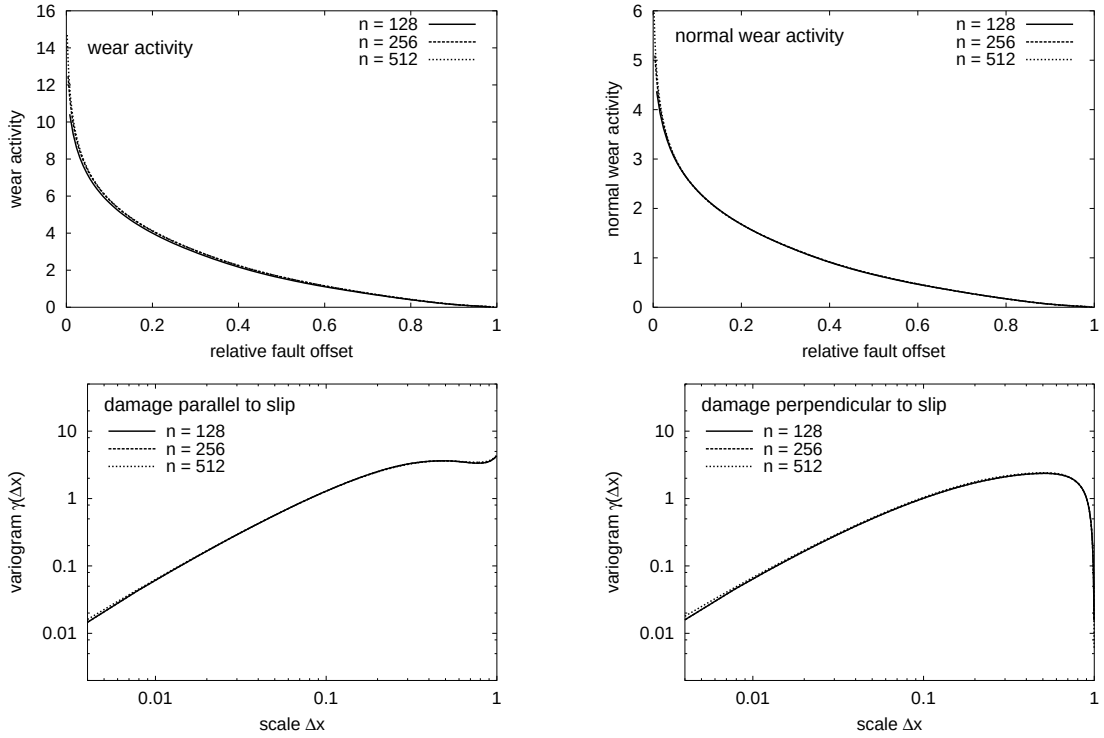

Fig. 5.9: Model behavior for different grid sizes.

5.6.3 Variation of relative strain

Variation of mean relative strain δ has almost no relevance to damage, neither for wear activity, nor for the scaling of damage (Figure 5.10). High values of δ should increase the contact area and stimulate damage. Yet, there is no significant influence of the mean relative strain. This indicates that the effect of wear to increase contact area outranges the effect of the mean relative strain. Indeed, if wear is reduced by setting α to high values ($\alpha = 80$), a slight influence of δ can be noticed (Figure 5.11).

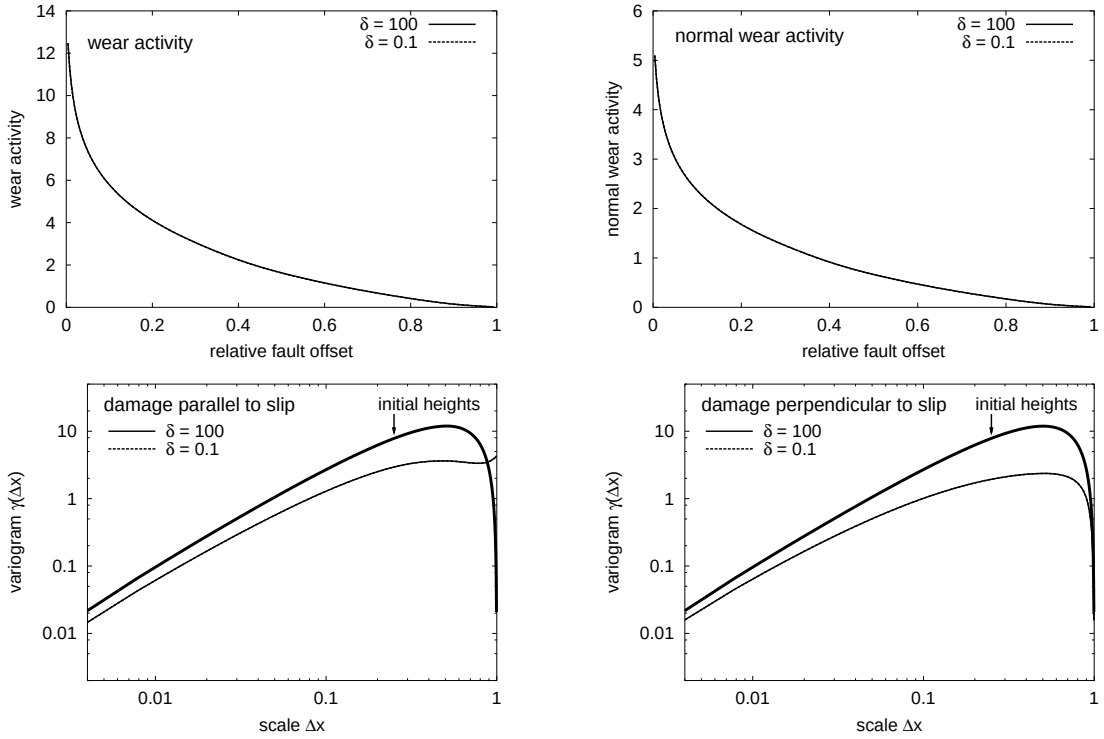

Fig. 5.10: Model behavior for a relative strain of 0.1 (small contact area) and 100 (large contact area).

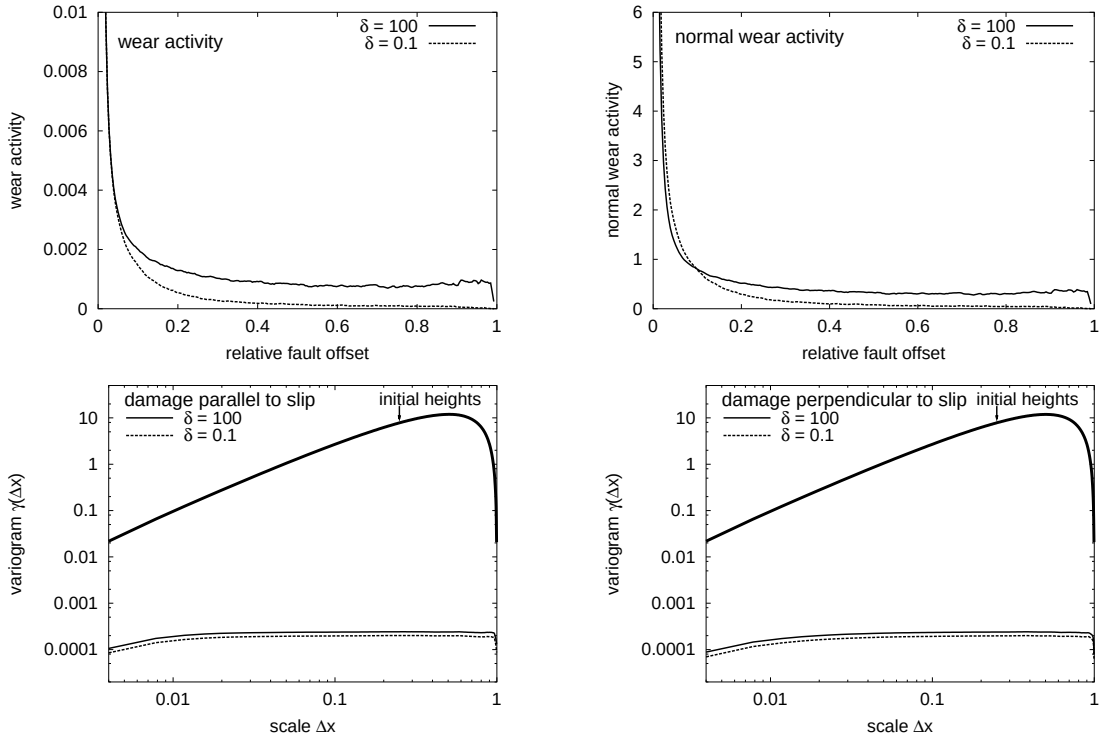

Fig. 5.11: Model behavior for a relative strain of 0.1 (small contact area) and 100 (large contact area) if fault adaption due to damage is suppressed by $\alpha = 80$.

5.6.4 Variation of relative yield slope

There is a strong influence of relative yield slope α on the wear process (Figure 5.12). The amount of damage is highest if α is small, i.e. if the rock is soft or the roughness amplitudes are high (see wear activity). Also, wear activity holds on longer for small α. This is an interesting result since there are two competing processes which influence the duration of wear activity. For small α, wear activity should drop off fast due to the fast decrease of roughness amplitudes. On the contrary, fault surfaces are able to adapt to each other better if the relative yield slope is low; this increases the contact surface and promotes wear. Apparently, the second process has greater relevance to the wear process.

Also the scaling of the damage field is sensitive to the relative yield slope. Large wavelengths evolve faster if high relative yield slopes are small. As a consequence, the final wear field will show relatively more small-scale structures for high values of α.

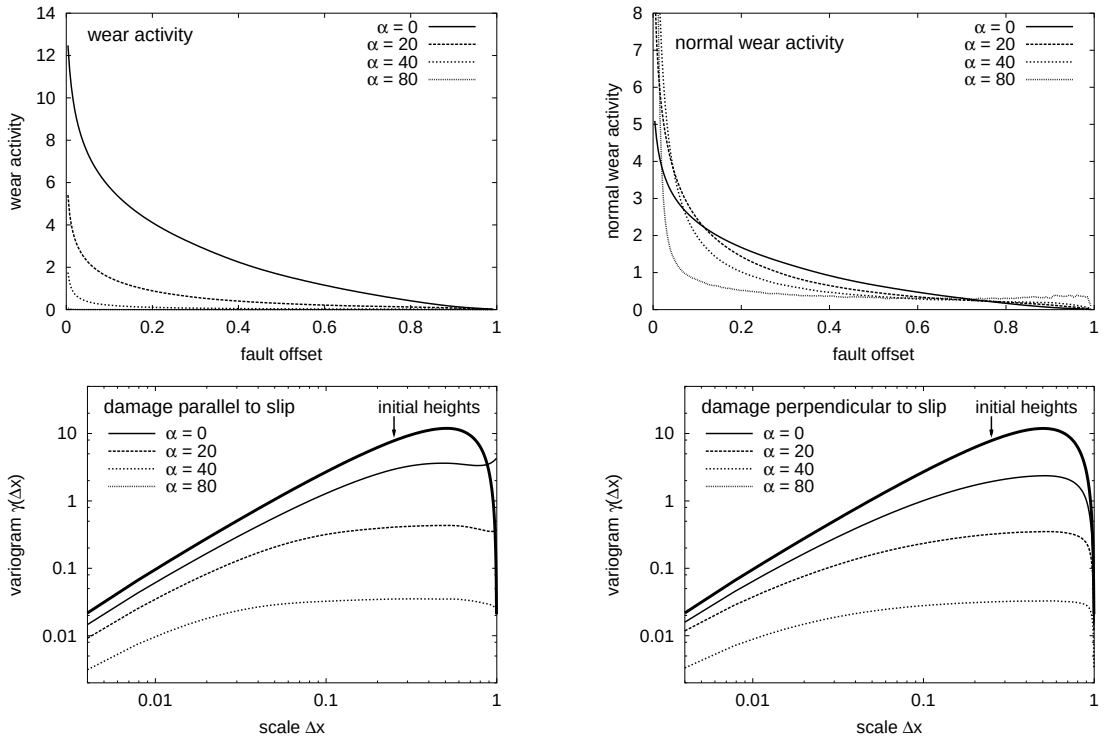

Fig. 5.12: Model behavior for different relative yield slopes.

5.6.5 Variation of Hurst exponent

Since the roughness of the wear field tries to approach the roughness of the surface heights, the scaling of the initial fault topography has an immediate influence on damage (Figure 5.13). According to the variograms, the roughness of the damage field increases together with the roughness of the initial fault surface. Wear activity drops off faster for rough fault surfaces because rough surfaces have low amplitudes at large scales.

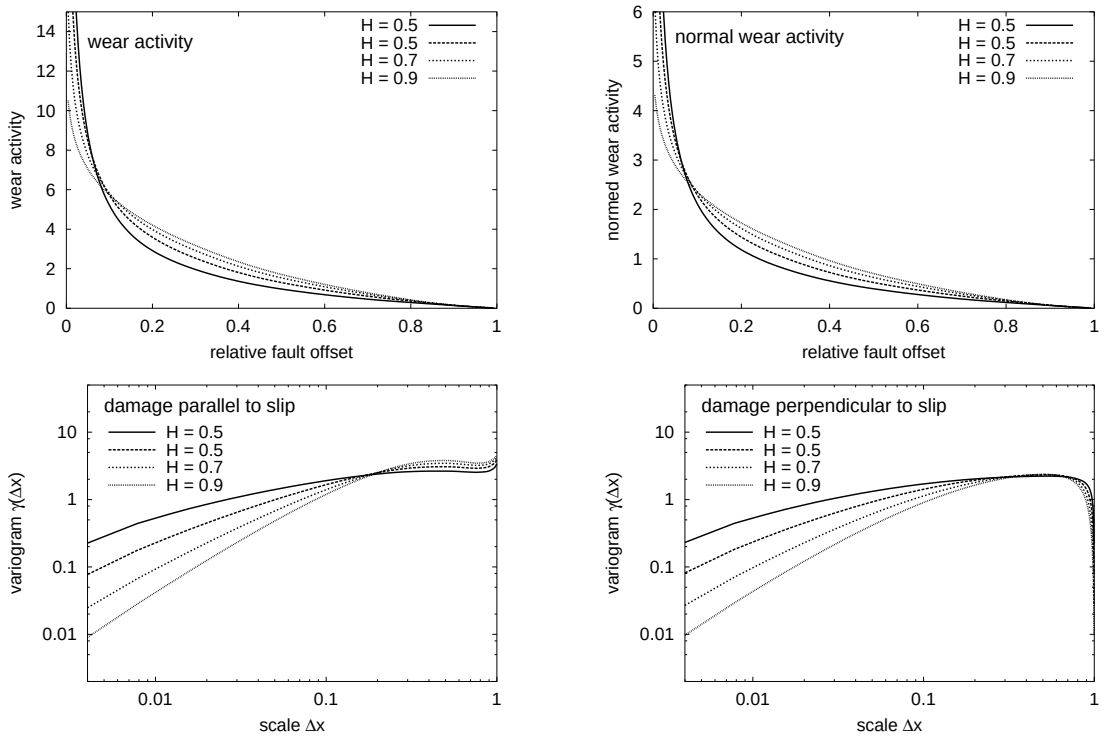

Fig. 5.13: Model behavior for different Hurst exponents.

5.6.6 Variation of lubrication

Figure 5.14 shows the model behavior if the detached material is removed from the fault gouge. The wear activity clearly shows the effect of lubrication: the lubricant reduces the amount of wear and causes a rapid drop off of wear activity. Thus, lubrication is an important factor for the evolution of the damage.

If damage is accelerated by removal of the lubricant, the anisotropy of the damage field increases (Figure 5.14 bottom). A possible reason for asymmetry is that damage scale grows more slowly perpendicular to slip. However, the variograms show that the damage field approaches a different scaling for both directions. Parallel to slip, the scaling of damage tends towards the scaling of the initial surface because fault surfaces are flattened by wear. Of course, this state cannot be reached due to the limited fault size. Perpendicular to slip, the absolute roughness of the damage field exceeds that of the initial fault surface at small scale. Thus, the scaling of damage does not converge against the scaling of the initial fault surface. According to Figure 5.15, the high roughness of the damage field at small scale is attributed to a lineation which is superimposed on the isotropic roughness inherited from the initial fault topography. Thus, there seems to be a general anisotropy of the damage field.

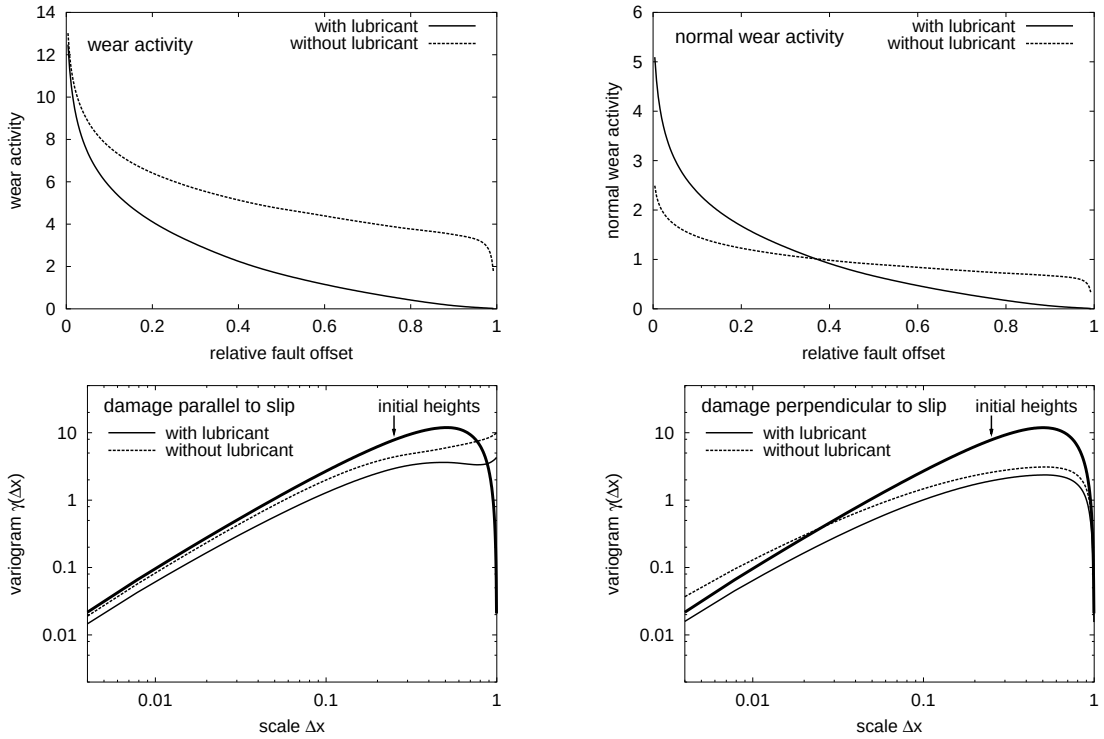

Fig. 5.14: Model behavior with and without removal of detached material.

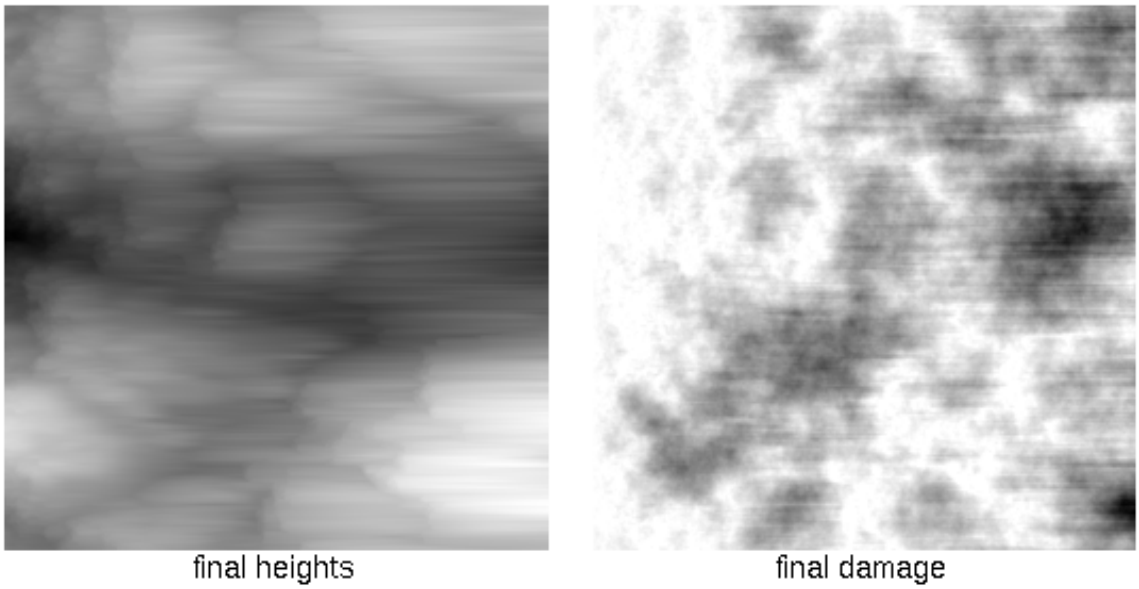

Fig. 5.15: Final topography and damage field of the lower plate if lubricant is removed from the fault gouge.

5.6.7 Comparison with field and experimental data

The numerical model simulates damage due to the displacement of rough fault surfaces on the basis of stable creep and minimal damage necessary for fault slip. Although the underlying physics is simple and the model behavior is mainly driven by the fracture geometry, the results fit to natural phenomena quite well:

- **Striation**. The numerical model reproduces striation and residual pull apart structures typical also for natural slip surfaces. The sharp ends of the lineations point in direction of motion. Striation produces a strong smoothening of fault surfaces in slip direction. This might explain why vertical roughness is so difficult to detect in the field: very large outcrop scales have to be inspected to find deviations from cylindrical fault geometry. The model indicates that damage may still take place even if there is no obvious vertical roughness visible in the field. The damage process will diminish but never cease because fault surfaces are always rough at scales larger than fault offset.
- **Characteristic scales of damage**. The multi-scale analysis of fault traces has shown that damage scale increases with fault offset. This phenomenon is reproduced by the

numerical model as a consequence of displacing surfaces with a multi-scale roughness. Fault offset has a major influence on the degree of surface mismatch at a given scale: surface correlation is high for scales much larger than fault offset and low for scales much smaller than the offset. Indeed, for zero offset, opposing positions of the fault surfaces are fully correlated on all scales since both surfaces have identical topography. For a certain wavelength of roughness, mismatch should be greatest if fault offset is approximately equal to half of the wavelength (this can readily be seen if roughness is considered as a sine-function). This is the reason why damage develops first at small scales during slip.

- **Wear loss**. The numerical model produces high wear loss if the area of surface contact is increased either by increasing the mean relative strain δ or by decreasing the relative yield slope α. This corresponds to increasing normal stresses and decreasing shear strength. Both is known to enlarge the real area of surface contact (Logan and Teufel 1996, Scholz 1990). In the model, wear activity decreases gradually with fault offset because asperity heights are reduced by wear. This is in good agreement with the results of wear experiments performed by Wang and Scholz (1994) who observed a similar drop off of wear loss during displacement for unmated rough surfaces in Westerly granite.

Apparently, numerical model and field observations draw a uniform picture of damage and fault surface evolution during fault offset. Since the model behavior is essentially controlled by the topography of the fault surfaces, roughness is probably an important parameter for natural damage processes, too.

5.7 Discussion

It was mentioned that fault topography gets smoother in slip direction during fault offset. This behavior is a simple consequence of the wear process. On the contrary, fault surfaces have some freedom to develop perpendicular to slip, since roughness in this direction provides no obstacle for slip in the model. Indeed, it can be noticed that roughness perpendicular to slip develops in a somehow surprising way. For a given scale, roughness amplitudes in slip direction do not exceed the amplitudes of the initial surface heights because the process of minimal wear tries to establish a plane surface. This is not the case perpendicular to the slip direction. Here, roughness amplitudes are achieved that are higher than the initial surface heights.

Two processes can explain the evolution of roughness perpendicular to slip: Every elevated asperity with a scale greater than fault offset is in frictional contact with its counterpart

on the adjacent surface. Both asperities suffer damage and are ”eroded” by friction. In this way, the isotropical roughness of the initial fault surface is transferred to the roughness of the damage field, which in turn is isotropical, too. The situation is different for asperity scales much smaller than fault offset. In this case, fault surfaces are highly uncorrelated, and there is a raised probability that two asperities under frictional contact are not in exact opposition to each other but have an offset perpendicular to the slip direction. This causes lateral abrasion of asperities and induces that asperities get narrower perpendicular to the slip direction, thereby increasing the roughness on smaller scales. By way of lateral abrasion, roughness can exceed the initial roughness of the fault surfaces because small wavelengths inherit the amplitudes of large wavelengths. The presence of a lubricant counteracts this process because it separates the fault blocks with the consequence that only large wavelengths of roughness, which have high amplitudes, get the chance of frictional damage. Therefore, the effect is only visible if the lubricant is removed in the model.

We can summarize that, on a given scale, there are two competing processes modifying roughness perpendicular to slip: roughness amplitudes are reduced by wear and, on the other hand, increased by the scale transfer of roughness amplitudes. Apparently, the geometry of fault surfaces alone is capable of causing a damage behavior that cannot easily be predicted since the influence of both competing processes is unknown. The system is free to develop roughness perpendicular to slip. The self-organization of roughness in this direction is maintained as long as there is a permanent input of large-scale roughness during fault growth.

Chapter 6

Conclusions

6.1 Fault evolution and scale interaction

The field observations allow to distinguish two stages of fault evolution that are characterized by different processes: a first stage of fault nucleation without significant fault slip and a second stage with considerable amount of slip (a single propagating fault contemporarily shows both stages at the central and fringe parts). In the pre-slip stage, processes like fracture coalescence and non-planar fault propagation create rough fault surfaces partly due to material inhomogeneities and stress asymmetry. In the slip-stage, damage structures are formed by friction. For scales below 10 m, the multi-scale analysis indicates an increase of damage scale with fault offset. The results of the numerical model confirm that characteristic scales of damage should occur as a consequence of multi-scale roughness and fault offset. Since damage alters the fault, fault formation appears to be a process that endures as long as a fault is active.

The mentioned change of faulting processes in the course of fault evolution corresponds to a change of scale coupling characteristics (in the meaning of structure interaction). The pre-slip stage is governed by mechanical interaction of fractures resulting in the formation of larger fractures. This is the process of fault nucleation. In the slip-stage, an additional mechanism of scale coupling is introduced by friction on rough fault surfaces. The numerical model suggests that damage owing to fault roughness is not a scale-invariant process: in the model, damage is controlled by the relative yield slope, a parameter that depends on roughness amplitude, cohesion and internal friction angle; all of these parameters are scale dependent in nature. Consequently, damage need not produce similar structures at different scales. Summarizing these findings, we notice upward and downward directed scale coupling processes that control the organization of multi-scale patterns.

Although multi-scale patterns are produced, this does not imply a continuous spectrum of fracture scales. Indeed, damage due to fault roughness was found to generate fractures and shear zones at scales well below the fault size so that there is a gap between the size of the largest damage structure and the fault itself. The continuity of fracture scales is important for the intensity of interaction between fractures of different size, i.e. for the intensity of scale coupling (in a qualitative sense). Interaction between fractures is strongest if sizes are similar, i.e. if there is a continuous spectrum of structure sizes. In case of a discontinuous size spectrum, strain is highly concentrated and few large fractures dominate the system behavior. It is clear that the behavior of a fracture network is easier to predict if the degree of strain concentration is high.

Faults show variations in the continuity of structure scales. According to the field observations, the continuity of structure sizes depends on observation scale and location. Shear strain appears to be well concentrated at map scale where single faults are visible. Thus, we find a discontinuous scale spectrum here (main fault; large splay faults at the 100 m scale; damage at scales below 10 m). On the contrary, if faults are inspected in the field, shear strain appears to be weakly concentrated at some locations, for example, at broad zones of fragmentation. Here, we find a continuous spectrum of fracture scales. This may change again if even smaller scales are considered. Due to the relation between continuity of spectra and intensity of scale coupling, we can expect that the intensity of scale coupling also varies with scale and location, and probably also with time. This clearly demonstrates the complexity of the system.

Whether a fault appears as an assembly of structures with continuous or discontinuous scale spectrum depends on the considered scale. Different scale ranges must be considered for different fault properties of interest. Dependent on the objective, a fault is either an assembly of fractures with similar or strongly differing sizes. This results in different approaches in characterizing fault properties that will be discussed briefly in the next chapter.

6.2 Friction and slip dynamics

Hallgass et al. (1997) have shown that faults with fractal surface topography could be able to induce a power-law distribution of earthquake moments with statistics similar to the well known Gutenberg-Richter law (Gutenberg and Richter 1954). Yet, fractal earthquake statistics can also be a self-organized behavior caused by stick-slip (Bak and Tang 1989). Slider-block models for fault slip, firstly introduced by Burridge and Knopoff (1967) and basing on the stick-slip assumption, produce distributions of earthquake moments which partly reproduce the Gutenberg-Richter law.

Stick-slip occurs in materials which exhibit velocity weakening. Static friction coeffi-

cients have to exceed the dynamic friction coefficients to allow the driving forces to accelerate the rock and produce a sliding instability (Rabinowicz 1965). Many materials show velocity weakening effects. Even in unconsolidated granular rock, which does not support large stick-slip movements due to dilatancy hardening, small stick-slip events can be observed at low velocities (Nasuno et al. 1998, Chain et al. 2001). Similar effects can be observed in lattice-solid model of sheared granular fault gouge (Mora et al. 2000). Stick-slip even occurs between atomically smooth mica (Demirel and Granick 1996) and ion crystals (Mitchell et al. 2001).

The roughness of fractures and faults is known to influence rock friction and hence stick-slip motion. Yet, it must be noted that this is only one of many processes relevant for rock friction. The idea that friction is influenced by the roughness of material contacts is old and reaches at least back to 1699 when Amontons formulated his two laws of rock friction. Frictional forces increase with growing area of surface contact. Mechanical processes at asperity contacts therefore strongly influence the static as well as the dynamic friction coefficient. Elastic deformation, brittle failure or plastic flow of asperities increase the real contact area, and the two latter sign responsible for the increase of friction coefficients with time (Dieterich 1972). Friction coefficients in natural rock exceed the value of $\frac{1}{6} \approx 1.5$ predicted for plastic material by the adhesion theory of friction (Bowden and Tabor 1950, 1964) due to asperity interactions. These involve ploughing of grooves, shearing through asperities, and sliding up of asperities (Scholz 1990). When these processes are suppressed, low friction coefficients are observed. Byerlee (1967), for instance, measured low friction coefficients ($0.2 < \mu < 0.6$) for very smooth sliding surfaces. Friction coefficients also decrease, if sliding-up is suppressed by inhibiting fracture dilatancy by means of high pressure. This provides an explanation why Byerlee (1978) measured friction coefficients around 0.85 at low loads whereas friction coefficients of 0.6 occurred at high loads. The influence of asperity interactions is also demonstrated by the large variation of friction coefficients in the measurements of Byerlee (1978) at low pressures which is attributed to the stronger influence of asperity interaction and to natural variations in surface roughness.

It is observed, that a critical slip distance has to be overstepped to trigger a slip instability. This can partly be explained by the fact that the correlation of rough surfaces in contact is reduced by slip (Scholz 1988). Consequently, the area of contact and the friction coefficient should show slip-dependence. Frictional strength can recover after the slip event due to failure or flow of asperity tips and consequent increase of contact area (Dieterich 1978). Thus, roughness is able to introduce a velocity weakening effect that promotes stick-slip.

This brief introduction should have pointed out the importance of fault roughness for slip dynamics. In the following, we summarize the results of the study which are of relevance to friction and stick-slip:

- **Characteristic scales of friction**. The characteristics of fault friction should change as fault roughness is modified in the course of fault offset. The numerical model has shown that the scale of striation grows during slip thereby introducing characteristic scales of roughness. The smoothening of fault surfaces at scales well below the fault offset suggest a decrease of friction coefficients in this scale range. Asperity interaction should be stronger at scales higher than fault offset leading to raised friction coefficients.

- **Efficiency of asperity failure**. Although the observed splay faults are probably induced by interlocking asperities they do not provide efficient slip surfaces to override the obstacle. The phenomenon of splay faulting shows that damage at interlocked asperities need not immediately create new slip surfaces which are suitable for slip. Thus, a broad rock volume can be affected by damage before slip takes place. The dilatancy caused by straining a fragmented rock body may cause strain hardening that counteracts velocity weakening. Thus, asperity failure must not necessarily imply the onset of a slip instability.

- **Spatial fluctuation of slip events**. Damage due to fault roughness leads to a continuous widening of the shear zone. Not the entire shear zone must be involved in slipping. If there is a broad zone of damage, slip surfaces are allowed to organize within a large rock volume. Such a spatial fluctuation of slip events can be observed in the lattice-solid model of Mora et al. (2000) for shear of a granular fault gouge between rough contacts. Due to material inhomogeneities, friction coefficients of natural faults may vary with the location of the slip event.

- **Influence of roughness perpendicular to slip**. In nature, roughness perpendicular to slip should be relevant to dynamical slip processes because a slip surface performs at least small movements perpendicular to the mean slip direction. It was shown, that perpendicular roughness can develop high amplitudes at small scales by narrowing of asperities; so even small movements perpendicular to the mean slip vector are facing a rough fault topography. Thus, striation should have an effect on friction and, by implication, on slip dynamics. Since slip also modifies striation, there is an interaction between fault topography and slip dynamics.

Chapter 7

Relevance for the approach to complex geosystems

7.1 On recognizing and monitoring geosystems

Complex geosystems are multi-scale systems and therefore cannot be recognized as a whole. No human mind and no computer can recognize the vast amount of particles present in a geosystem at a time. So how can we recognize complexity at all? In fact, descriptions of geosystems in geo-sciences and geo-engeneering often neglect the multi-scale aspect where it should be taken into account.

A geosystem provides certain *phenomena* at certain scales. An inherent property of a phenomenon is that an observer always has the possibility to search for constitutive objects. A fault, for instance, is formed by an arrangement of grains; grains again are formed by an arrangement of minerals and pore space, and so on. If we think of a fault, there are always only few constitutive elements we consider and many which we do not even think of. In other words, a phenomenon is an abstract quality because we always abstract from constituents except for few. We can speak of a ”multi-scale system”, but this term does not comprise very much: it needs further specification concerning the ingredients at different scales. It is not really true that we recognize the entire system and isolate phenomena (like certain objects) as semantical units. Phenomena are all that we have at disposal to approach the invisible thing, which is the complex system. We can therefore understand a complex geosystem as a compilation of phenomena that are tightly related to each other, mostly by structural similarity or conditional relationship. In case of faulting, we notice that faults of different size influence each other and therefore seem to belong to a common system, which as a whole stays invisible. The phenomenon of complexity is the phenomenon that a multi-

scale search will reveal ever new related aspects. Thus, if we do not search at several scales, we will not notice complexity. Recognizing a single fault, for instance, does not necessarily include the awareness that we deal with a complex geosystem.

This study was addressed to the role of fault roughness for scale coupling. Considering mechanisms of scale coupling may stimulate the search for other relevant system scales. This is especially important for field surveys where observers are always bound to a very limited range of observation scales. Monitoring geosystems must apply multi-scale technics to find the scales that are relevant to the system.

7.2 On modeling geosystems

Not all scales of a geosystem need to be of relevance. Which scales must be considered depends on the system property that is of interest. This property might only be controlled by a limited range of system scales. If we want to measure fault offsets, it is usually sufficient to consider the largest faults. On the contrary, if fluid permeability is of interest, many system scales have to be considered because even minor discontinuities can have significant influence on flow paths. There is no model of a geosystem which can consider all system scales, but it might be possible to cover the scale range that is relevant to the system property that is of interest. Only in this case, models are able to provide results that reflect natural processes (Fig. 7.1).

Whether a geosystem establishes a continuous or discontinuous spectrum of object scales is of relevance to the scale range that can be spanned by a model. Under the aspect of scale-continuity, existing numerical models of multi-scale systems can be categorized into two general types:

- *Models with continuous space or time scales* are based on process descriptions at the scale of grid cells or time steps, i.e. at a microscopic scale. It is possible to extend the scale range at which processes are formulated by use of adaptive grids or variable time steps. In principle, these models can have the ability to represent continuous scales of spatial or temporal patterns. Classical examples for this model type are slider-block models for fault slip, mainly represented by the *Olami-Feder-Christensen (OFC)* model and its derivates, which establish a continuous scale spectrum of slip events (Olami et al. 1992, Jensen 1998). A disadvantage of models with continuous pattern scales is the requirement of large computational resources. Thus, large scale ranges are realized at the expense of scale resolution and vice versa.

- *Models with discontinuous space or time scales* consider processes at separated scale domains. Mechanisms of scale coupling between adjacent scale domains are formu-

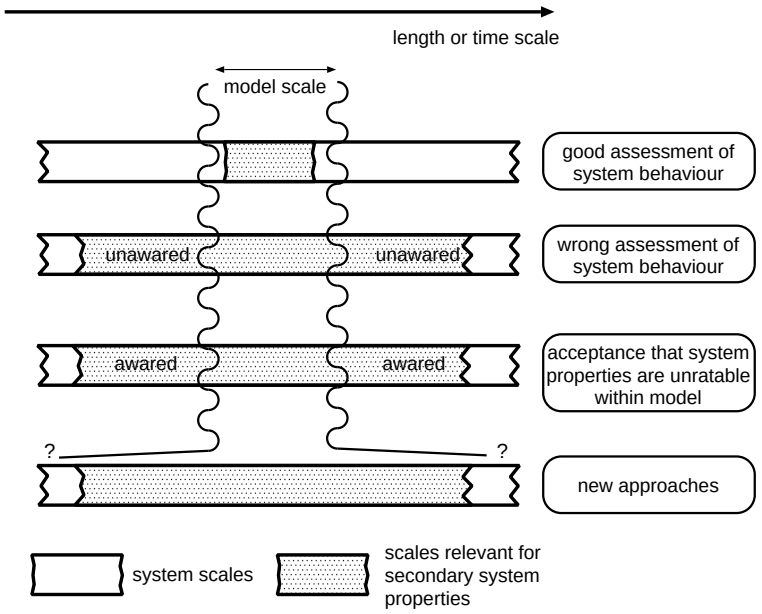

Fig. 7.1: Assessment of modeling approaches for complex systems.

lated. Scale coupling can introduce scale interaction or uni-lateral control by one process scale. An example for this model type is the fault model introduced in this study. Here, fault slip is described at a macro-scale whereas damage is assumed to be a process at a micro-scale. Changes on the micro-scale are controlled by the macro-scale by means of fault roughness. Important for models with discontinuous scales is the existence of scale domains at which spatial or temporal patterns cannot be represented. In the fault model of this study, scale ranges are strictly separated because damage cannot produce any structural pattern on the macro-scale. Thus, models with discontinuous space or time scales inhibit self-organization of patterns between the represented scale domains. On the other hand, they are able to consider large scale ranges together with a high scale resolution at the scale domains of interest.

Models with discontinuous space or time scales are only applicable if there is a scale for which there is a representative description of small-scale processes (”parameterization”), i.e. a representative elementary volume (”REV”). This requires that scale coupling is independent from pattern formation at intermediate scales that are not represented in the model. The existence of intermediate patterns inhibits a representative description of the lower scale domain. In this case, models with continuous space or time scales have to be applied at the cost of scale range or scale resolution.

Models with discontinuous scale spectrum can be applied to faults if there is a high degree of localization. It was mentioned before that the degree of localization of a fault depends on scale and location. Models with continuous spectrum of scales have to be used at scales where interaction of fractures produces patterns with continuous scale distribution. Today, all numerical models that allow continuous scales of fractures to describe the evolution of such fracture networks fight the restriction of limited computational resources.

7.3 Can we understand geosystems?

The matter of complexity has so many faces that an answer to this question can only reflect a personal opinion. Deciphering processes acting in a geosystem is surely not enough to really *understand* a geosystem. It would be more satisfying if the system behavior could be forecasted due to the knowledge of such processes. Whether this is possible or not depends on the width of the relevant scale range. If we, for example, know how secondary structures are induced by fault roughness, we might be able to forecast the damage along a single fault, but this does not enable us to forecast the behavior of a rock volume covering a multiplicity of scales and faults, even if this was the only relevant process. So, knowing processes does not imply that we are able to forecast the system's behavior. Especially, if scale interaction introduces feedback to the system, we have to quantify the system's state at many scales to make a good forecast; and this is probably impossible in most cases.

Numerical models are of help to make forecasts for a multi-scale system. Yet, the self-organized behavior of the models is often far away from being traceable by the human mind. Such models provide an understanding in terms of a statistical prediction of the system behavior in dependence of model parameters, but they do not clearly show how these predictions are determined by the driving processes. Thus, there seems to be a black spot between driving processes and the behavior of a complex system. This actually is the reason why there is need to speak of *emergence*.

Bibliography

Bak, P. and C. Tang (1989). Earthquakes as a self-organized critical phenomenon. J. Geophys. Res., 94:15,635–15,637.

Barabaasi, A.-L. and H. Stanley (1995). Fractal Concepts in Surface Growth. Cambridge University Press, Cambridge.

Bouchaud, E. (1997). Scaling properties of cracks. J. Phys.: Condens. Matter, 9:4319–4344.

Bouchaud, E., G. Lapasset, and J. Planès (1990). Fractal dimension of fractured surfaces: a universal value? Europhys. Lett., 13(1):73–79.

Bowden, F. and D. Tabor (1950). The friction and lubrication of Solids. Part I. Clarenden Press, Oxford.

Bowden, F. and D. Tabor (1964). The friction and lubrication of Solids. Part II. Clarenden Press, Oxford.

Brown, S. (1987). Fluid flow through rock joints: the effect of surface roughness. J. Geophys. Res., 92(B2):1337–1347.

Brown, S. and C. Scholz (1985a). Broad bandwidth study of the topography of natural rock surfaces. J. Geophys. Res., 89(B15):12,575–12,582.

Brown, S. and C. Scholz (1985b). Closure of random elastic surfaces in contact. J. Geophys. Res., 90(B7):5531–5545.

Brown, S. and C. Scholz (1986). Closure of rock joints. J. Geophys. Res., 91(B5):4939–4948.

Burridge, R. and L. Knopoff (1967). Model and theoretical seismicity. Seis. Soc. Am. Bull., 57:341–371.

Byerlee, J. (1967). Theory of friction based on brittle fracture. J. Appl. Phys., 38:2928–2934.

Byerlee, J. (1978). Friction of rocks. Pure Appl. Geophys., 116:615–626.

Chain, R., N. Page, and S. Biggs (2001). Microsopic and macroscopic aspects of stick-slip motion in granular shear. Phys. Rev. E, 64:016413/1–8.

Childs, C., A. Nicol, J. Walsh, and J. Watterson (1996). Growth of vertically segmented normal faults. jsg, 18(12):1389–1397.

Demirel, A. and S. Granick (1996). Friction fluctuations and friction memory in stick-slip motion. Phys. Rev. Lett., 77(21):4330–4333.

Develi, K. and T. Babadagli (1998). Quantification of natural fracture surfaces using fractal geometry. Mathematical Geology, 30(8):971–998.

Dieterich, J. (1972). Time dependent friction in rocks. J. Geophys. Res., 77:3690–3697.

Dieterich, J. (1978). Time dependent friction and the mechanics of stick slip. Pure Appl. Geophys., 116:790–806.

Feder, J. (1988). Fractals. Plenum Press, London, New York.

GLA (1988). Geologie am Niederrhein. Geologisches Landesamt NRW, Krefeld.

Gutenberg, B. and C. F. Richter (1954). Seismicity of the Earth and Associated Phenomenon. Princeton Univ. Press, Princeton, 2nd ed.

Hallgass, R., V. Loreto, O. Mazzella, G. Paladin, and L. Pietronero (1997). Earthquake statistics and fractal faults. Phys. Rev. E, 56(2):1346–1356.

Halpin-Healey, T. and Y.-C. Zhang (1995). Kinetic roughening phenomena, stochastic growth, directed polymers and all that. aspects of multidisciplinary statistical mechanics. Physics Reports, 254:215–414.

Hansen, A., J. Schmittbuhl, G. Batrouni, and F. Oliveira (2000). Normal stress distribution of rough surfaces in contact. J. Geophys. Res. Lett., 27(22):3639–3642.

Jensen, H. J. (1998). Self-Organized Criticality – Emergent Complex Behaviour in Physical and Biological Systems, vol. 10 of Lecture Notes in Physics. Cambridge Univ. Press, Cambridge.

Journel, A. G. and C. Huijbregts (1978). Mining Geostatistics. Academic Press, London, New York.

Klinkenberg, B. (1994). A review of methods used to determine the fractal dimension of linear features. Mathematical Geology, 26(1):23–46.

Lee, J. and R. Bruhn (1996). Structural anisotropy of normal-fault surfaces. jsg, 18:1043–1059.

Lehner, F. and W. Pilaar (1997). The emplacement of clay smears in synsedimentary normal faults: inferences from field observations near Frechen, Germany – in: P. Møller-Pedersen (editor): Hydrocarbon Seals - Importance for Exploration and Production. Elsevier, Amsterdam, New York.

Logan, J., C. Dengo, H. Higgs, and Z. Wang (1992). Fabrics of experimental fault zones: their development and relationship to mechanical behaviour. In: B. Evans and T.-f. Wong (editors): Fault Mechanics and Transport Properties of Rock. Academic Press, New York.

Logan, J. and L. Teufel (1996). The effect of normal stress on the real area of contact during frictional sliding in rocks. Pure Appl. Geophys., 95:471–86.

López, J. and J. Schmittbuhl (1998). Anomalous scaling of fracture surfaces. Physical Review E, 57(6):6405–6408.

Malinverno, A. (1999). A simple method to estimate the fractal dimension of a self-affine series. Geophys. Res. Lett., 17(11):1953–1956.

Måløy, K., A. Hansen, and W. Roux (1992). Experimental measurements of the roughness of brittle cracks. Phys. Rev. Lett., 68(2):213–215.

Mandel, J., L. de Jong, and A. Maltha (1977). Shear zones in granular material. Rock Mech., 9:95–144.

Mandelbrot, B. (1967). How long is the coast of britain? statistical self-similarity and fractional dimension. Science, 165:636–638.

Mandelbrot, B., D. Passoja, and A. Paullay (1984). Fractal character of fracture surfaces of metals. Nature, 308:721–722.

Mandl, G. (1988). Mechanics of Tectonic Faulting. Elsevier, Amsterdam.

Mandl, G. (2000). Faulting in Brittle Rock. Springer, Heidelberg.

McAnulty, P., L. Meisel, and P. Cote (1992). Hyperbolic distributions and fractal character of fracture surfaces. Physical Review A, 46:3523–3526.

Mitchell, T., J. Bollinger, W. Itano, and D. Dubin (2001). Stick-slip dynamics of a stressed ion crystal. Phys. Rev. Lett., 87(18):183001/1–4.

Moore, D. and D. Lockner (1995). The role of microcracking in shear-fracture propagation in granite. jsg, 17(1):95–114.

Mora, P., D. Place, S. Abe, and S. Jaume (2000). Lattice solid simulation of the physics of fault zones and earthquakes: the model, results and directions. in: Geophysical Monograph 120, GeoComplexity and the physics of Earthquakes. American Geophysical Union.

Nasuno, S., A. Kudrolli, A. Bak, and J. Gollub (1998). Time-resolved studies of stick-slip friction in sheared granular layers. Phys. Rev. E, 58 (2):2161–2171.

Olami, Z., H. J. S. Feder, and K. Christensen (1992). Self-organized criticality in a continuous, nonconservative cellular automation modeling earthquakes. Phys. Rev. Lett., 68:1244–1247.

Patton, T., J. Logan, and M. Friedman (1998). Experimentally generated normal faults in single-layer and multilayer limestone specimens at confining pressure. Tectonophysics, 295:53–77.

Peacock, D. (1991). Displacement and segment linkage in strike-slip fault zones. Journal of Struct. Geology, 13:1025–1035.

Peacock, D. and D. Sanderson (1991). Displacements, segment linkage and relay ramps in normal fault zones. Journal of Struct. Geology, 13:721–733.

Poon, C., R. Sayles, and R. Jones (1992). Surface measurement and fractal characterization of naturally fractured rocks. J. Phys. D: Appl. Phys., 25:1269–1275.

Power, W., T. Tullis, S. Brown, G. Boitnott, and C. Scholz (1987). Roughness of natural fault surfaces. Geophys. Res. Lett., 14(1):29–32.

Rabinowicz, E. (1965). Friction and wear of materials. John Wiley, New York.

Rice, J. (1983). Constitutive relations for fault slip and earthquake instabilities. Pageoph, 121:443–475.

Rudnicki, J. (1988). Physical models of earthquake instability and precursory processes. Pageoph, 126:531–554.

Schmittbuhl, J., S. Gentier, and S. Roux (1993). Field measurements of the roughness of fault surfaces. Geophys. Res. Lett., 20:639–641.

Schmittbuhl, J., F. Schmitt, and C. Scholz (1995). Scaling invariance of crack surfaces. J. Geophys. Res., 100(B4):5953–5973.

Scholz, C. (1987). Wear and gouge formation in brittle faulting. Geology, 15:493–495.

Scholz, C. (1988). The critical slip distance for seismic faulting. Nature, 336:761–763.

Scholz, C. (1990). The mechanics of earthquakes and faulting. Cambridge Univerity Press, Cambridge, New York.

Scholz, C., N. Dawers, J.-Z. Yu, and M. Anders (1993). Fault growth and fault scaling laws: preliminary results. J. Geophys. Res., 98(B12):21,951–21,961.

Segall, P. and D. Pollard (1980). Mechanics of discontinuous faults. Journal of Geophysical Research, 85(B8):4337–4350.

Seidel, J. and C. Haberfield (1995). Towards an understanding of joint roughness,. Rock Mech. Rock Engng., 28(2):69–92.

Shen, B., O. Stephansson, H. Einstein, and B. Ghahreman (1995). Coalescence of fractures under shear stresses in experiments. J. Geophys. Res., 100:5975–5990.

Skempton, A. (1966). Some observations on tectonic shear zones. Proc. 1st Congr. Int. Soc. Rock. Mech. Lisbon, 1:329–385.

Wang, W. and C. Scholz (1994). Wear processes during frictional sliding of rock: A theroretical and experimental study. J. Geophys. Res., 99(B4):6789–6799.

Watterson, J., C. Childs, and J. Walsh (1998). Widening of fault zones by erosion of asperities formed by bed-parallel slip. Geology, 26:71–74.

Willemse, E. and D. Pollard (1998). On the orientation and patterns of wing cracks and solution surfaces at the tips of a sliding flaw or fault. J. Geophys. Res., 102(B2):2427–2438.

Willemse, J. (1996). 3D Mechanics and evolution of discontinuous faults. Ph.D. thesis, Stanford University, Standford, Calif.

Yang, Z. and G. Chen (1999). Application of the self-affinity concept to the scale effect of joint roughness,. Rock Mech. Rock Engng., 32(3):221–229.